Analytical and Experimental Validation for DC Arc Flash Models

by

Corey Steven Weimann

Bachelor of Science in Engineering, Electrical Engineering, University of Pittsburgh, 2018

Submitted to the Graduate Faculty of the

Swanson School of Engineering in partial fulfillment

of the requirements for the degree of

Master of Science in Electrical and Computer Engineering

University of Pittsburgh

2020

UNIVERSITY OF PITTSBURGH

SWANSON SCHOOL OF ENGINEERING

This thesis was presented

by

Corey Steven Weimann

It was defended on

July 9, 2020

and approved by

Masoud Barati, PhD, Assistant Professor, Department of Electrical and Computer Engineering

Mohamed Bayoumy, PhD, Assistant Professor, Department of Electrical and Computer Engineering

Alexis Kwasinski, PhD, Associate Professor, Department of Electrical and Computer Engineering

Thesis Advisor: Brandon Grainger, PhD, Eaton Faculty Fellow, Department of Electrical and Computer Engineering

Thesis Advisor: Robert Kerestes, PhD, Assistant Professor, Department of Electrical and Computer Engineering

Analytical and Experimental Validation for DC Arc Flash Models

Corey Steven Weimann, M.S.

University of Pittsburgh, 2020

With the utilization of DC systems increasing, and constant emphasis for worker safety is a top priority for all companies, arc flash feasibility for DC systems is a growing concern. Current literature providing background information regarding AC and DC arc flash, including its importance are presented. In addition, this article details the feasibility of DC arc flash events with experimental scouting tests for a 130 VDC system. Sensitivity studies are experimentally performed on the impact of bus gap distance and bolted fault current level on incident energy. Test results are analyzed and conclusions drawn on the results in particular incident energies. Details of the tests performed including the setup, procedure, and system parameters are also provided. Additionally, theoretical methods of determining incident energy for the testing conditions are explored. Specifically, these are Doan's and NFPA 70E's maximum power models, and Stokes and Oppenlander's and Paukert's arc resistance models. A comparative analysis of the test results to industry standard, NFPA 70E, and software analysis methods using ETAP, an industry leading software used for arc flash studies, is performed.

Table of Contents

List of Tables

List of Figures

Acknowledgments

I would like to thank my parents, Cynthia Weimann and William Weimann III, for their support and guidance throughout this process. I would also like to thank William Weimann III from Wabtec Corporation for acquiring the copper for the bus work, as well as, spending many hours machining all the insulators and bus work used for testing. The testing would not have been possible without the help of Roy Ball, Emmanuel Munguia, and Michael Lang from Mersen, and I thank them for providing lab use, and assistance with the test setup and testing. I would like to thank Eric Grant and Santino Graziani from Eaton Corporation for providing the cable tray, mechanical lugs, and cable for the testing. I would also like to thank Dr. Masoud Barati, and Dr. Mohamed Bayoumy, for serving on my committee. Lastly, I would like to thank Dr. Robert Kerestes, and Dr. Brandon Grainger for advising me through this entire process, and giving me this opportunity.

Nomenclature

Acronym	Description
HCB	horizontal electrodes inside a metal enclosure
HOA	horizontal electrodes in open air
MCC	motor control center
NEC	National Electrical Code
NFPA	National Fire Protection Association
OSHA	Occupational Safety and Health Administration
PPE	personal protective equipment
PV	photovoltaic
VCB	vertical electrodes inside a metal enclosure
VCBB	vertical electrodes terminated in an insulating barrier inside a metal enclosure
VOA	vertical electrodes in open air

1.0 Introduction

Arc flash, as defined by [1], is "an electric arc event with thermal energy dissipated as radiant, convective, and conductive heat." The electric arc can form, due to equipment malfunction or failure, poor operation and maintenance, tools dropped while energized, tools left in equipment during de-energized maintenance, animals, and poor electrical connections that cause a fault to occur and allow current to flow through the air. Arc flash events release heat, pressure, sound, light, and shrapnel. Depending upon the severity, this can injure or kill workers that are not properly protected with the appropriate PPE. In the US from 2012 to 2016, 739 workers died from exposure to electricity [2] (due to the way the injuries are recorded it is impossible to tell how many of these fatalities were caused by arc flash versus electric shock).

Protecting workers from arc flash is required by OSHA in Regulations 29 CFR 1910 [3] and 1926 [4], which requires employers to provide appropriate PPE, and safeguards from hazards. In addition, the NEC in Article 110.16 [5], requires equipment to be labeled to warn workers of potential arc flash hazards "before examination, adjustment, servicing, or maintenance of the equipment." Even if a company's policy is to only interact with equipment when de-energized the equipment must still be labeled. A worker's first step is to verify absence of voltage, which requires the worker to interact with the equipment, and the equipment may not have been de-energized as the worker presumed. This practices requires the equipment to be labeled so workers can don the appropriate PPE before interacting with the equipment.

To help meet the requirements required by law, there are standards that may be followed to assist employers in enacting and practicing safe electrical procedures. The foremost standards being IEEE Std 1584 – *IEEE Guide for Performing Arc-Flash Hazard Calculations*, [1], and

NFPA 70E *Standard for Electrical Safety in the Workplace*, [6]. IEEE 1584 provides insight into the calculation of the incident energy that a worker could be exposed to in an arc flash event. The standard provides equations to estimate the incident energy that were empirically derived from approximately 2,000 three-phase AC tests with its revision in 2018. The standard, however, excluded single-phase AC and DC systems. NFPA 70E establishes requirements and guidelines to address the safety of employees exposed to electrical hazards, in particular, interacting with energized equipment, in order to create a safe environment for employees either performing maintenance or general workplace electrical safety practices.

Due to the exclusion of DC systems in IEEE 1584, NFPA 70E is left to address DC arc flash electrical hazards. However, unlike the equations developed in IEEE 1584 for three-phase AC systems, the equations in NFPA 70E are theoretical and were not supported with testing.

DC arc flash testing and the results are limited in public literature. The most notable testing was performed by Kinectrics [7] which found that the NFPA 70E/maximum power method was over-conservative. More recently, testing was performed by EPRI [8] with a PV power supply which found the NFPA 70E/maximum power method was about 3 to 10 times higher than their measured results.

For this work, testing was performed at 130 VDC in an attempt to confirm the incident energy results obtained from NFPA 70E and ETAP [9], an industry leading software tool for arc flash analysis, and to determine if there is a minimum available short circuit fault current where an arc flash event could no longer occur. Prior tests did not use vertical electrodes terminated in an insulating barrier inside a metal box / enclosure (VCBB) electrode configuration, as used during this testing. For DC system evaluation, it was presumed that the benefits for increased energy

results, and observable increases in low voltage sustainability in AC tests with the VCBB configuration would also be applicable for DC tests.

In Section 2.0, background information is provided on AC (Section 2.1) and DC (Section 2.2) arc flash. The DC arc flash experimental testing performed and results are reported in Section 3.0. The testing setup and testing procedures are detailed in Section 0. In Section 3.2, the experimental results are presented. In Section 3.3, the theoretical models with the parameters of the experimental testing are used to calculate the estimated incident energy. In Section 0, the incident energies measured during testing are compared to the estimations from the theoretical models. Finally, in Section 4.0, conclusions are drawn based upon the results of the testing.

2.0 Arc Flash

Arc flash phenomenon in electrical power systems was first addressed concerning life safety of workers in 1982 with work performed by Lee [10].

Since his work there has been the development of IEEE Std 1584 – *IEEE Guide for Performing Arc-Flash Hazard Calculations*, in 2002 [11], which provided insight into the calculation of the incident energy that a worker could be exposed to in an arc flash event. The standard provided equations to estimate the incident energy that were based on empirical results from approximately three-hundred (300) three-phase AC tests, however, the standard excluded single-phase AC and DC systems from the standard.

In 2018, the standard was revised to incorporate approximately two-thousand (2,000) tests. With the additional testing, the equations for calculating the incident energy were revised, the range of the model extended, and additional electrode configurations were added to better model actual electrical equipment. Even with the extensive revision, single-phase AC and DC systems are still excluded from the standard.

When workers may be exposed to arc flash hazards an arc flash analysis must be performed. Today, AC arc flash studies are performed in most industrial facilities with power system analysis software such as ETAP [9], SKM [12], EasyPower [13], etc. However, DC systems are typically not addressed, due to the non-standardization of determining the possibility or the level of hazard of DC arc flash. Since IEEE 1584 does not address DC arc flash, NFPA 70E is the leading resource in providing insight on DC arc flash hazard analysis. However, these insights are based on theoretical models and not testing as was done in IEEE 1584 for three-phase AC systems.

2.1 AC Arc Flash

2.1.1 Maximum Power Method

As mentioned above, Lee produced one of the first models/methods to estimate arc incident energy [10] which was based on the maximum power the arc could achieve and the maximum energy that could be released by the arc and exposed to a worker.

The maximum power, in watts, is the system voltage times one-half the bolted fault current. The arc energy was represented as a sphere radiating uniformly outward with a diameter as a function of the square root of the arc power. Reference [10] stated that some arcs may be lower than the maximum, but the maximum possible estimation must be considered for the protection of the worker. In [10] it was discovered that the energy exposure from the arc is inversely proportional to the square of distance. Therefore, as a worker's distance from the arc increases the energy absorbed by the worker is reduced drastically.

In addition, [10] also explored the temperatures and duration of exposure that resulted in curable and incurable burns of human skin. The maximum energy from the arc (based on the system parameters), the distance from the arc, and the limits of the human skin before incurable burns would occur (without considering any heat reflection from the skin to reduce heat exposure), were combined into a relationship with the following equations:

$$D_C = \sqrt{2.65 \times MVA_{bf} \times t} \qquad (2-1)$$

$$D_f = \sqrt{1.96 \times MVA_{bf} \times t} \qquad (2-2)$$

Where,

D_C distance for a curable burn (ft)

D_f distance for a fatal burn (ft)

MVA_{bf} bolted fault MVA at point involved

t time of exposure (s)

In the future with AC arc flash testing, to develop IEEE 1584, it would be found that this method is generally very conservative, but this estimation was revolutionary at the time providing some of the first insights into AC arc flash and the risk it posed to worker safety. Some examples of the problems with this method are presented in [14], and some of the key findings are detailed below.

Using curable and incurable burns as the results of equations (2-1) and (2-2) rather than incident energy, resulted in additional assumptions and simplifications that further affected accuracy of the results. For example, it was later found that the absorption of skin is actually around 0.94 to 0.99, thereby making the assumption that the human skin absorption coefficient neared one (ie. all absorbed) incorrect, making the point of incurable burns closer to the arc than a more realistic case with some of the energy being reflected by the skin.

In addition, the method of determining the severity of burns based on the duration of exposure and skin temperature rise for determining heat exposure was found to be inaccurate in [15]. Lee's use of maximum power transfer resulting in the power of the arc being one half the

maximum power of the bolted fault was later found to be much higher than reality. From experimental testing for IEEE 1584 – 2002 the average power was only 33.2% of the maximum power, much lower than the 50% estimated/used by Lee.

2.1.2 Electrode Configurations

As stated, the IEEE 1584 revision added additional electrode configurations to better model electrical equipment. Originally the standard only considered the VOA (vertical electrodes in open air), Figure 1, and the VCB (vertical electrodes inside a metal enclosure), Figure 2, configurations. In the 2018 edition the HOA (horizontal electrodes in open air), Figure 1, HCB (horizontal electrodes inside a metal enclosure), Figure 2, and VCBB (vertical electrodes terminated in an insulating barrier inside a metal enclosure), Figure 2, configurations were added.

Reference [1] provides some guidance on selection of appropriate electrode configurations for electrical equipment. For faults in panelboards, disconnect switches, MCC buckets and internal to their circuit breakers, switchgear with the circuit breaker not racked in all of the way, and the line side of a circuit breaker it was recommended that the VCBB configuration be used. For faults in the bus compartment of an MCC, load side of fuses and circuit breakers, and internal faults of switchgear power circuit breakers a VCB configuration is recommended. The HCB configuration is recommended for faults in switchgear compartments without the power circuit breaker inserted and fuse clips. VOA and HOA electrode configurations are recommended for exposed transformer terminals depending on the blast direction relative to the worker. If the blast is directed directly at the worker the horizontal configuration should be used.

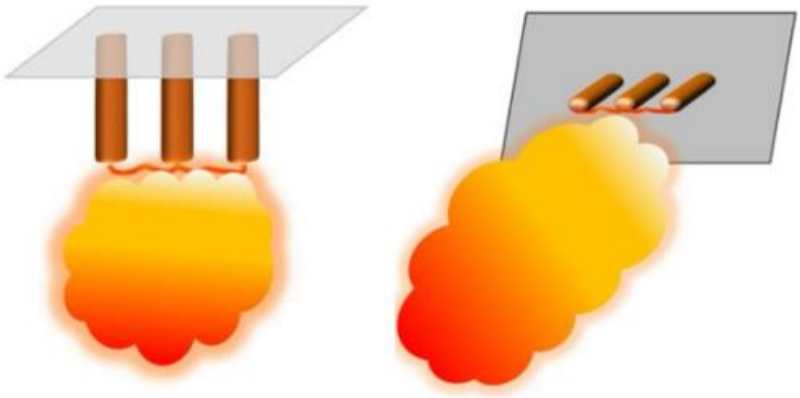

Figure 1 VOA (left) and HOA (right) Configurations [16].

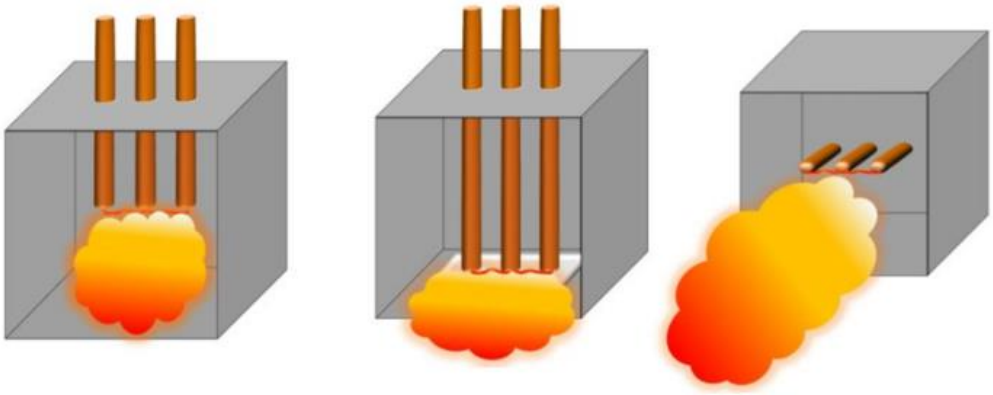

Figure 2 VCB (left), VCBB (middle), and HCB (right) Configurations [16].

2.1.2.1 Electrodes in a Metal Enclosure

Additional AC arc flash analysis of the IEEE 1584 2002 edition tests were performed in [17], the standards testing results were found to correlate well, $r^2 = 0.95$, with electrodes in a VOA configuration. However, when the arc was enclosed, now a VCB configuration, the results were less accurate with a correlation of only 0.78. Reference [17] determined that the walls of the open-

front enclosure reflected some of the radiant heat equally in all directions resulting in additional radiant heat being directed out of the enclosure opening, towards the worker. These reflections resulted in a focusing/intensifying effect, increasing the incident energy measured at the working distance. Using view factors, based on the size of the enclosure, [17] modified the 2002 IEEE 1584 equation to yield:

$$E_{max} = 84.61\,\{E_S + F_R(\alpha)\,W_{ARC}\}^{0.958}\,g^{0.284}\,V_{LL}^{-0.532} \qquad (2-3)$$

Where,

E_{max} mean maximum energy density at a distance d (cal/cm^2)

E_S spherical component of energy density (J/mm^2) = $W_{ARC}/(4\pi d^2)$

W_{ARC} total arc energy computed using the time domain model (J)

$F_R(\alpha)$ reflected view factor (mm^{-2})

The reflectivity α was determined, via correlation with test results, to be about 0.56, meaning that the reflected radiant heat energy accounts for over half of the total radiant incident energy seen by the worker for arc flashes occurring in an enclosure.

AC arc flash testing in enclosures was also performed in [18], and based on initial testing, found that having the arc in an enclosure could increase the incident energy by up to three times, when compared to open air. However, it was also found that the disparity between the open air and enclosure results decreased as the bolted fault current decreased. In addition to the incident energy increase, it was observed that the arc voltage decreased, for arcs in an enclosure, when

compared to open air. Implying that the arc resistance decreases and arcing current increases when the arc is in an enclosure.

Through high-speed imaging it was seen that a plasma cloud was projected from the box with its size and severity increasing with the bolted fault current. This plasma cloud caused convective heating transfer to the calorimeters in addition to the typical radiant heat energy from the arc. Arcs are generally 90% radiant energy, but when enclosed the convective property appeared enhanced adding additional heat transfer to the calorimeters, as stated in [18]. Due to the plasma cloud and enhanced convective heating, [18] found that the relationship between incident energy and distance from the arc was lessened. As discovered in [10], the energy exposure from the arc is inversely proportional to the square of distance, however, due to the additional convective heating, the impact of the distance from the arc was decreased. This resulted in increased incident energies farther from the arc when compared to arcs in open air. In summary, when an arc is enclosed, the incident energy leaving the enclosure is higher and will decrease less rapidly as the distance from the arc is increased.

It was assumed that the focusing affect and increase in incident energy would be similarly applicable for DC systems. Therefore, the testing, detailed in Section 3.0, was performed in an enclosure to increase the incident energy levels that could be seen in the event of a successful arc flash event.

2.1.2.2 AC Arc Flash Testing with VCBB Configuration Findings

Tests in enclosures for the IEEE 1584 – 2002 standard were originally done with a VCB configuration, which allowed an arc to form from the tips of the electrodes and cause arc blasts to shoot into the bottom of the enclosure. The arc cloud then fills the enclosure and is ejected out of the open front of the enclosure. This method however does not represent the worst case incident

energy since the plasma cloud is being directed down then out of the enclosure. It is argued that the HCB would result in the worst case incident energy since the cloud is directed directly outward towards the worker. This configuration is not very representative of most electrical equipment, but would represent bus stabs, fuse clips, etc. as stated earlier. Reference [19], presents that the VCBB configuration more closely represents the majority of electrical equipment due to the fact that the electrical conductors are generally terminating into a protective device or other device, such as power distribution blocks, circuit breakers, terminal blocks, etc., that would impede the downward formation and direction of the arc resulting in a similar plasma cloud action as the HCB configuration.

Testing was performed in [19] at a high power laboratory with system voltages of 208 to 600 V, the bus gap distances ranged from 0.5 to 2 in, and bolted fault currents of 4.5 to 45 kA. Testing with these parameters was performed 235 times, with 144 of the tests using the VCBB configuration. From the VCBB test results, it was concluded that when compared to the VCB configuration, on average; the arcing current increased by about 20%, incident energy increased by about 31%, and the arc length decreased about 26% resulting in a decrease of arc voltage. These results had greater disparity as the testing voltage increased. In addition, it was discovered in [19] that the plasma cloud was directed outwards just above the insulating barrier from high-speed imaging of the plasm cloud, and the heat distribution of the calorimeters (with the middle row being 52% higher than the mean, compared to the bottom row being 32% higher than the mean with VCB configuration).

Due to the overall decrease in arc length, arcing voltage and resistance, and increase in arcing current, it can be seen that the VCBB configuration provided a stabilizing effect. This stabilization also allowed low voltage arc flash test to be more sustainable. Testing performed in

[19] at 208 V could not sustain arcs below 10 kA bolted fault current in the VCB configuration, but were sustainable with the VCBB configuration. It was concluded in [19] that the HCB configuration could be used to represent the worst case incident energy due to its easier and less costly testing, when compared to VCBB. However, VCBB allows for more sustainability of arcs at low voltages, and should be used for testing with sustainability concerns and low voltage testing.

It was assumed that the increased sustainability and incident energy when using the VCBB configuration for AC testing would still be applicable for DC systems. Therefore, the testing, detailed in Section 3.0, was performed in a VCBB configuration to increase the likelihood of successful arc flash events at the low voltage, and increase the incident energy levels of successful arc flash events.

2.2 DC Arc Flash

When comparing AC vs DC arc flash, there are no zero crossings for DC, unlike AC, resulting in increased difficulty of current interruption. In addition, the arcs tend to be higher energy compared to AC due to the energy expended for re-striking at every zero crossing for AC [14]. In addition, DC arc flash events depend heavily on their source as seen in PV systems, and some of the sources have very limited supply such as batteries. DC arc flash incident energy estimation can be broken up into approximately three categories; maximum power, based on the maximum power operating point of an electric arc, arc resistance, based on estimating the arc geometry and resistance based on previous arc testing, and PV systems, based on the non-linear I-V characteristics of PV array sources.

2.2.1 Maximum Power Method

With no real estimates for DC arc flash incident energy Doan introduced a method to conservatively estimate the incident energy in 2010 [20]. Doan developed equations for incident energy of DC arcs by using the maximum power of the arc. This method has become the most commonly accepted method for determining DC arc flash incident energy, and was adopted in NFPA 70E [6] for DC incident energy calculations and by the National Electrical Safety Code [21].

This method's approach is very similar to [10] for AC arc flash and pulled many similarities and conclusions for the development of the DC version. By assuming steady state conditions, system inductance can be neglected, leaving only the system and arc resistances. This assumption makes calculations easier and results in a more conservative incident energy because the inductance would only decrease the maximum power of the arc. Using this assumption, and the maximum power transfer theorem, the maximum power of the arc as presented in [20] would be:

$$P_{max} = \frac{\left(\frac{V_{sys}}{2}\right)^2}{R_{sys}} \qquad (2-4)$$

Where,

P_{max} maximum power of the arc (W)

V_{sys} system voltage (V)

R_{sys} system resistance (Ω)

Then, the energy at the maximum power of the arc, (2-4) is multiplied by time. The time is the clearing time of the arcing fault (time taken to interrupt the fault). In DC systems the time constant has a large impact on the clearing time. With time constants below 10 ms the operation is similar to AC fuse curves, but time constants above 10 ms deviate considerably and take much longer to clear compared to the AC fuse curves due to the slow increase in fault current [20]. Considering the arc energy to be a sphere, radiating equally in all directions, as done in [10], and using the working distance to determine the surface area of the sphere, the incident energy can be calculated using:

$$IE_{\max power} = 0.005\left(\frac{V_{sys}^2}{R_{sys}}\right) * \frac{T_{arc}}{D^2} \qquad (2-5)$$

Where,

$IE_{\max power}$ estimated incident energy at the maximum power point (cal/cm^2)

T_{arc} arcing time (s)

D worker's distance from the arc (also known as working distance) (cm)

Reference [20] stresses that this method is a preliminary assumption of incident energy estimation, and further research/testing needs to be performed to further quantify the results of DC arc flash. This estimation may be lower than what actually occurs. For example, the arcing fault could be lower than the maximum arcing fault current and the time to clear could become great enough that it would have a higher incident energy than the maximum power point arcing current and its clearing time. Reference [20] recommends multiplying by a factor for arcs in an enclosure, which would seem prudent based on the findings in [17] and [18] for AC arc flash tests in

enclosures. However, no specific method or value to adjust the overall incident energy for DC arcs in enclosures are provided. NFPA 70E – 2015 [22] recommends multiplying by a factor of three for arcs in an enclosure, based on the findings in [18] of arcs in enclosures, resulting in a maximum of 3 times the incident energy than open air (as already discussed in Section 2.1.2 for AC arc flash). However, this factor is worst case and changes based on system parameters, such as electrode configuration, fault current, voltage, enclosure size, gap distance, etc.

This method also assumes complete transfer of electrical energy to radiant heat energy, which is inaccurate. Some energy will be used for pressure increase, light, sound, etc. and will not cause only radiant heat energy that is exposed to the worker, as stated in Section 1.0. This assumption leads to potentially higher incident energy estimations, requiring additional unnecessary PPE burdening maintenance personnel.

In addition, as stated in [14], "Accurate estimation of the arc current is essential in determining the expected response time of the overcurrent protective device." The assumption of the arcing current being one half the bolted fault current, is not an accurate means for determining the arcing current and could lead to under estimation of the actual clearing time. If the arcing fault current is inaccurate, and leads to longer clearing times, the arc flash incident energy could become greater than the perceived worst case incident energy with the arc at the maximum power point. A longer duration lower fault current arc flash can have a higher incident energy than a shorter duration higher fault current arc flash.

The time constant (L/R) is also important for determining the response of protective devices, impacting the fault current rise and potentially delaying activation of the device, as illustrated in [23].

2.2.2 Arc Resistance Methods

As [24] summarized, most early testing of DC arcs were series arcs and performed at low current for the utilization of electric arcs for illumination. Some of this testing and subsequent arc models included: Ayrton, Steinmetz, and Nottingham, but these models/results did not provide or have detailed testing parameters and procedures. However, they were confirmed by testing performed later by Van and Warrington, and Miller and Hildenbrand. This confirmed that the arc voltage is proportional to the arc length, and that the I-V characteristic is inverse and non-linear at low currents, and at higher currents the arc voltage changes very little with a change in arc current.

Stokes and Oppenlander performed the most testing to develop I-V characteristics of series arcs (horizontal and vertical orientations) in open air, and is one of the leading models for the arc resistance method. Their testing determined that there is an inverse relationship between current and voltage at low currents, and a direct relationship between current and voltage at higher currents, Figure 3. The point at which this change in I-V characteristic, and at which the vertical and horizontal series electrode configurations had the same behavior due to the magnetic forces dominating the response, was called the transition point.

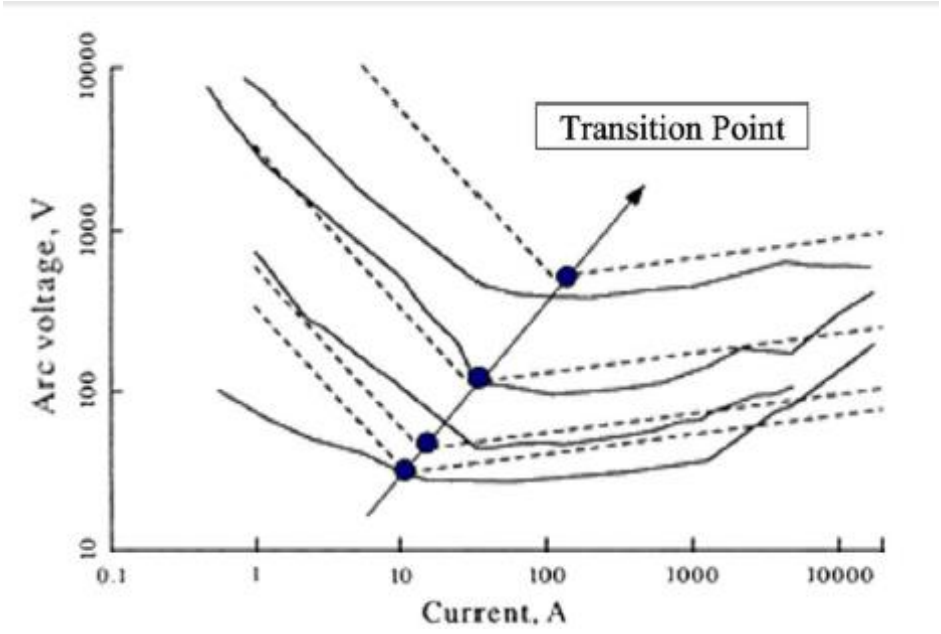

Figure 3 Arc I-V Characteristics [24].

(Solid line are measured values, and dashed lines are estimated from the instantaneous power equation (2-6).

The arc testing performed by Stokes and Oppenlander included both AC and DC systems [25], with horizontal and vertical series open air electrode configurations, with gap distances of 5 to 500 mm, and currents of 0.1 A to 20kA . From testing it was observed that the arc voltage experienced large and constant fluctuations, reaching up to four times the minimum value, while the current remained relatively constant throughout the duration of the test. The voltage fluctuations were attributed to the constantly changing physical arc geometry. The changing arc geometry was caused by thermal convection for low-current long duration arcs, and magnetic driven plasma jets for high-current short duration arcs. It is important to note that, due to the arc geometry changing, the gap distance does not equal the arc length.

The following equation in [25] was developed relating the instantaneous power of the arc to the transition current, current where the voltage reaches a minimum (inflection point or transition point of the arc I-V curve).

$$P(I) = \left(20 + 0.534 * z_g\right) I_t^{1.12} \qquad (2-6)$$

$$I_t = 10 + 0.2 * z_g \qquad (2-7)$$

Where,

I_t transition current (A)

$P(I)$ instantaneous power dissipated by arc (I > I_t) (W)

z_g electrode gap (mm)

In [25] it was discovered that there are two impacts that the self-created magnetic fields have on the arc formation and geometry. First, the current path from the electrodes to the main column to the arc is restricted, resulting in a high current density and therefore powerful magnetic field. The developed field drives the plasma jets away from the restriction and if the jets are not in the same direction as the shortest arc distance the arc will bridge the two jets together, that are away from the electrodes, increasing arc length. The second magnetic field is created from the current flowing through the electrodes, which acts on the main column of the arc and increasing the arc length.

The equations developed by Stokes and Oppenlander (2-6) and (2-7), were converted to an equation relating the arc resistance and current in [24].

$$R_{arc} = \frac{20 + 0.534 * z_g}{I_{arc}^{0.88}} \qquad (2-8)$$

Where,

I_{arc} arc current (kA)

R_{arc} arc resistance (Ω)

This relationship is more practical for using in arc flash incident energy estimation methods, due to its independence to the arbitrary transition current. However, a large drawback to utilizing this method is the need to iteratively solve (2-8) to determine the appropriate values of the arc resistance and current.

Paukert utilized laboratory results from seven researchers, with AC and DC tests, to develop arc voltage and arc resistance equations above and below 100 A (transition point) at a specified gap distance, and is considered the other main model for the arc flash resistance method. The results of Stokes and Oppenlander generally coincided with Paukert's findings, however, they did have some deviation especially for larger gap distances, and slight deviation around the transition point, Figure 4, as concluded in [24].

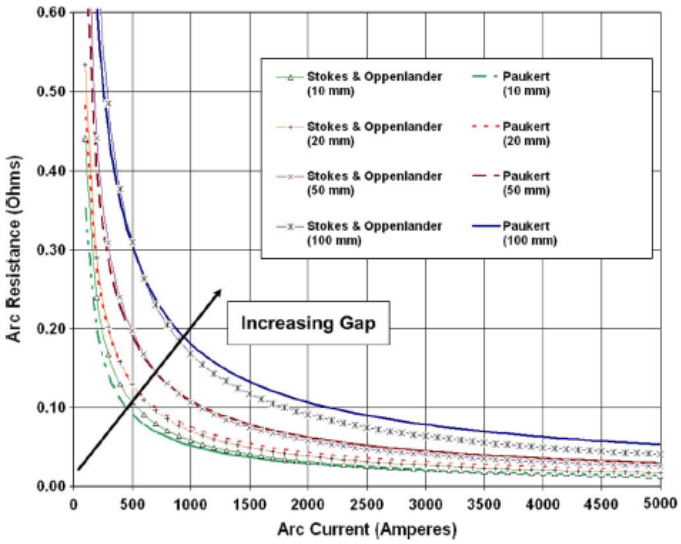

Figure 4 Comparison of Arc Resistance Equations from Stokes and Oppenlander's and Paukert's Testing at Varying Gap Distances [24]

The major drawback to the work performed by Stokes and Oppenlander, and Paukert is that the tests used as a basis for the models are based on series electrode configurations. Series electrode configurations would relate to protective device operation, while the parallel configuration would relate to what is seen in arc flash testing with phase (or opposite polarity) buses being shorted together or to ground. The parallel configuration unsurprisingly tends to have a higher arc length and subsequently higher arc voltage, due to the arc forming from end-to-end and electromagnetic forces pushing the arc downwards, as stated in [17] for VCB AC arc flash configurations. The series configuration tended to be the popular testing choice due to the popularity of testing for overcurrent protective devices and for illumination. However, this focus on series arc testing in early arc modeling makes it difficult to directly apply their results to DC arc flash which are largely parallel arcs.

2.2.3 PV Systems

For typical AC systems and battery supplied DC systems the fault current is typically magnitudes higher than the normal operating current allowing for the overcurrent protective device to detect and operate quickly under a fault condition to clear the fault. However, for PV supplied DC systems the fault current and operating current do not have the same separation, delaying the operation of overcurrent protective devices, particularly fuses. A typical PV array I-V curve can be seen in Figure 5, notice the small difference between the maximum power point current (9.0 A) and the short circuit current (9.5 A). As observed in [26], due to closeness of the short circuit current and maximum operating point (normal operating point) current, protective device operation may be delayed producing very long clearing times (greater than 2 sec). As stated previously, it is generally thought that a fault of a higher magnitude would yield higher incident energy, however, that is not always the case, and is reliant on the clearing time. A fault that has a higher current magnitude, but clears quickly, may not result in a higher incident energy than a fault at a lower current magnitude, but takes longer to clear. Therefore, [26] emphasized the importance of investigating where the fault current is high and instances that result in long clearing times when performing studies of PV arrays.

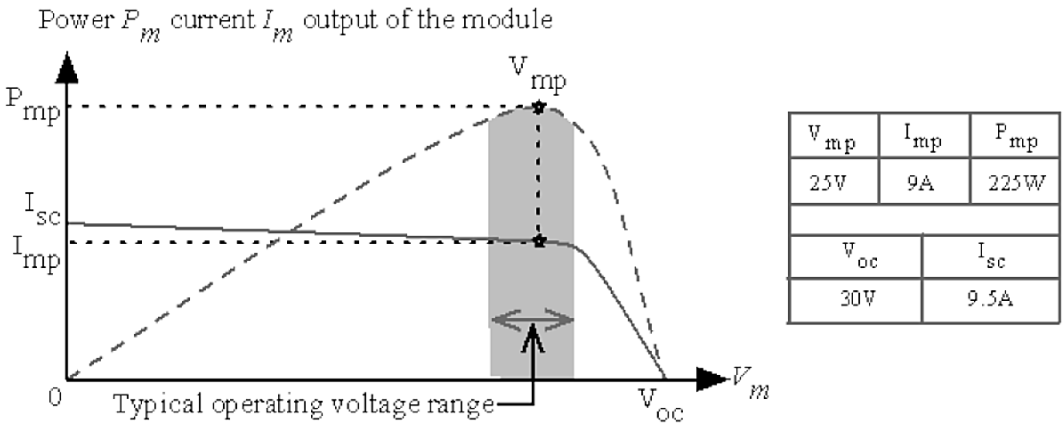

Figure 5 PV I-V Characteristic [27]

2.2.3.1 PV Array Arc Types

There are three types of arcs that can occur in PV systems; series, parallel, and ground arcs, as represented in Figure 6. The series arc would be an arc that forms on the current supply path of the positive lead (assuming the negative lead is grounded, the return path can be ignored). The parallel arc would be an arc that forms between two positive conductors. This type of arc would be minor or non-existent, due to the fact that the positive leads would be at approximately the same voltage. Lastly, the ground arc can be either a positive conductor to ground or to the negative conductor (also connected to ground). The ground arc has the largest voltage differential of the three arc types.

Intuitively, the more powerful arcs are likely to occur where the current is highest, which would be at the input of the inverter or at some point after the combiner boxes where the current from the PV array strings are combined. The inverter not only receives all of the current from the DC system, but also back-feeds current during ground faults adding additional current to the already high current from the DC system.

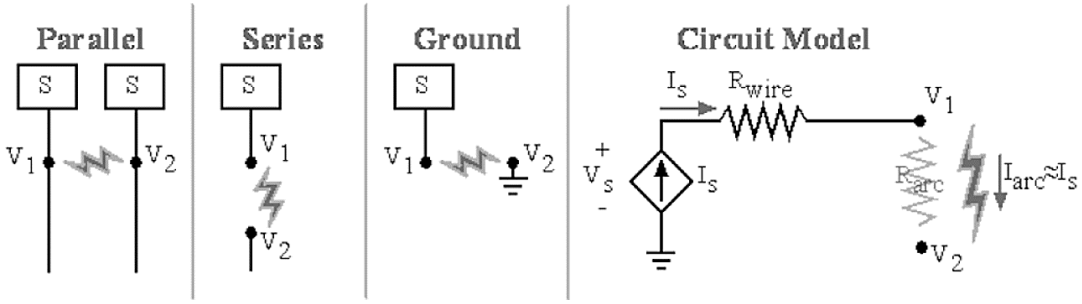

Figure 6 PV Arc Types and Circuit Model [27]

2.2.3.2 Arc Resistance Method

As seen in Figure 6 the PV array is modeled as a current source (typical for PV arrays), meanwhile battery systems are modeled as a voltage source. Due to the difference in I-V characteristics of PV systems compared to battery systems, the previous arc models discussed are not constructed for PV systems, this difference also carries into present DC arc flash calculation models which are based on a voltage source rather than a current source. To remedy this problem, [27] presented a new theoretical model to estimate incident energy for PV systems.

Using the circuit model in Figure 6, and assuming steady state, typical with most DC arc flash estimation models, it can be seen that the arc voltage is equal to the difference between V_1 and V_2. The arc voltage is also equal to the arc current times the arc resistance, the arc resistance is based on the Stokes and Oppenlander model [25]. The arc voltage and arc current are multiplied together to get the arc power, or the square of the arc current can be multiplied by the arc resistance to get the arc power. For ground arcs, V_2 is equal to zero since it is grounded, but for series arcs it is based on the voltage just before the arc occurs as shown in the equation below as presented in [27].

$$V_2 = V_{s_n} - I_{s_n} R_{wire} \qquad (2-9)$$

Where,

V_{s_n} prearcing normal source voltage (V)

I_{s_n} prearcing normal source current (kA)

R_{wire} resistance of the current path (**Ω**)

In order to calculate the incident energy of the arc the other electrical parameters need to be found, such as V_s. V_s can be calculated from (2-10), which is dependent on the value of V_1 and the voltage drop of the current path.

$$V_s = V_1 + I_s R_{wire} \qquad (2-10)$$

Where,

I_s source current (kA)

V_1 is based on the arc voltage and current. The arc current is the sum of the PV array strings' currents. The PV array current is based on the I-V characteristic of PV arrays, as seen in Figure 5. Therefore, the voltage of the arrays is needed to solve for the array current for a fixed load voltage. Iterative solving is required to obtain the arc properties (arc current and voltage). The iterative solving should continue until the arc current is sufficiently constant. Using the Stokes and Oppenlander based model for the arc resistance (2-8), the arc energy equation (2-11) (assuming all electrical energy is converted into thermal energy), and the incident energy radiating equally in all directions (2-12), results in the incident energy equation (2-13) as presented in [27].

$$E_{th} = I_{arc}^2 * R_{arc} * t_{arc} \qquad (2-11)$$

$$IE = 0.239 * \frac{E_{th}}{4\pi d^2} \qquad (2-12)$$

$$IE \approx 0.239 * \frac{\left(20 + 0.534 * z_g\right) * I_{arc}^{1.12} * t_{arc}}{4\pi d^2} \qquad (2-13)$$

Where,

E_{th} thermal energy released by an arc (J)

I_{arc} arc current (kA)

R_{arc} arc resistance (Ω)

t_{arc} arc duration (s)

d distance from arc (in open air) (cm)

IE incident energy (cal/cm^2)

z_g electrode gap (mm)

2.2.3.3 Maximum Power Method

Current standards, namely NFPA 70E use the maximum power transfer theorem developed in [20], as mentioned previously. For PV systems this method may prove to be ill-suited, due to its nonlinear I-V characteristic as seen previously in Figure 5. The voltage of the system is determined by the number of panels in series per string. The equations for the system voltage operating at the maximum power point, and open circuit (no-load condition) are provided in (2-14) and (2-15). The factor of two is representative of bipolar DC systems, common among solar farm installations. The current of the system is determined by the number of panel strings in parallel. The equations for the system current, operating at the maximum power point, and short circuit or bolted fault condition, are provided in (2-16) and (2-17) as presented in [28].

$$V_{mp-pv} = 2n_{s-pv}V_{mp} \quad (2-14)$$

$$V_{oc-pv} = 2n_{s-pv}V_{oc} \quad (2-15)$$

$$I_{mp-pv} = n_{p-pv}I_{mp} \quad (2-16)$$

$$I_{sc-pv} = n_{p-pv}I_{sc} \quad (2-17)$$

Where,

V_{mp-pv} system voltage at maximum power (V)

V_{oc-pv} system voltage at no-load or open circuit voltage (V)

V_{oc} PV module open circuit voltage (V)

V_{mp} PV module maximum power point voltage (V)

n_{s-pv} number of PV modules connected in series in a string

I_{mp-pv} system current at maximum power (A)

I_{sc-pv} system bolted fault current (A)

n_{p-pv} number of strings in parallel

I_{sc} PV module short circuit current (A)

I_{mp} PV module maximum power point current (A)

Assuming no losses in the system due to power distribution, the maximum possible power occurs at the maximum power point of the PV system. Therefore, the maximum arc power is based on this operating point, implying that the arc current is equal to the maximum power current (2-16), and the arc voltage is equal to the maximum power voltage (2-14). This implies that the maximum arc power is then equal to the product of (2-14) and (2-16).

To more accurately estimate the maximum power, the temperature effect on PV modules should be considered. As stated in [28], as the temperature decreases below 25°C the maximum power increases, and can increase by 25% in some cases at very low temperatures. Taking the maximum arc power (product of (2-14) and (2-16)) and multiplying it by the arc duration results in the maximum arc energy. Assuming the same equal energy dispersion (sphere) as [10] and [20], results in the maximum incident energy (2-18), with temperature compensation (2-19), as presented in [28].

$$IE_{max-pv} = 0.02 * V_{mp-pv} * \frac{I_{mp-pv} t_{arc}}{D^2} \qquad (2-18)$$

$$IE_{max-pv-comp} = IE_{max-pv} * \left(1 - \left(\frac{K_{T-Pmax}}{100}\right) * (25°C - T_{min})\right) \qquad (2-19)$$

Where,

D distance from arc (in open air) (cm)

IE incident energy (cal/cm^2)

K_{T-Pmax} temperature coefficient at maximum power (%/°C)

T_{min} lowest ambient temperature (°C)

Comparing (2-18) to the method in [20], [28] found that the incident energy of (2-18) was approximately three times higher than the maximum power method of [20]. This estimation was done using the average maximum power current and voltage, open circuit voltage, and short circuit current, from a survey of commercial utility-grade PV modules. The difference in using the maximum power equation developed by Doan [20] and the maximum possible power delivered by

the PV system is evident by this large disparity. This model also does not include any current back-feed from the inverter adding to the fault that would increase the incident energy further.

When comparing the methods presented in [27] and [28], large disparities between incident energies can be seen between the two methods. As observed in [29], the maximum power method developed in [28] (detailed in Section 0) does not depend on gap distance, its incident energy is fixed for a given system parameter. However, the arc resistance method in [27] (detailed in Section 2.2.3.2) is dependent on the arc length (due to the use of the Stokes and Oppenlander arc resistance equation), and therefore will vary when the bus gap distance is varied. In [29], it was seen that as the arc length was increased, the disparity between results decreased. For the example provided in [29], at a gap of 500 mm the incident energies were relatively close with the arc resistance method being slightly higher (about 10%) than the maximum power method. However, at a gap distance of only 10 or 20 mm the maximum power method is about ten times higher than the arc resistance method.

2.2.3.4 Additional Considerations for PV Systems

In addition to the non-linearity of PV arrays, additional variables that affect the operation of the arrays must be considered. PV array maximum power is variable and dependent on other factors including temperature, as stated, above, technological factors, and other meteorological / environmental factors. Solar panels experience a decrease in power when there is dust or snow covering the panel, but experience increase in power and open circuit voltage as irradiance increases. Cloud edge effect has also been reported in [26] to increase solar radiation by as much as 20%, and recommended its consideration when adjusting the maximum power due to environmental conditions. In addition, as stated in [28], a decrease in temperature causes an increase in open circuit voltage. However, [26] stated that the increase of voltage due to

temperature does not impact power as much as an increase in irradiance, and these typically do not occur at the same time. Some technological factors can increase the maximum power such as; positive power tolerance of panels during manufacturing, and inverter back-feed (varies by model and manufacturer). The age of the solar panel will have a negative impact on maximum power, and NREL found that the median decrease was around 0.5% per year [30].

2.2.4 Existing DC Arc Flash Testing

As stated, DC arc flash testing and the results are limited in public literature. The most notable testing was performed by Kinectrics [7] in Toronto. More recently, testing was performed by EPRI [8] with a PV power supply.

The DC arc flash testing by Kinectrics High Current Laboratory in Toronto was performed for Bruce Power and Coast Mountain Bus Company to provide an estimation method for DC arc flash exposures. The testing data was not released, but some published results from the testing can be found [7]. The testing consisted of 125 and 260 VDC, 1 to 25 kA bolted fault current, gap distances from 5 to 152.4 mm (0.2 to 6 in), clearing times of 0.01 to 2 s, working distances of 152.4, 304.8, 558.8, and 863.6 mm (6, 12, 22, and 34 in) (interestingly a 457.2 mm (18 in) working distance was not used which is typical for MCC, panelboards, and junction boxes per IEEE 1584), and VCB, VOA, HCB, HOA, and series electrode configurations.

The 600 V testing was performed with series electrodes in open air, HCB and VCB electrode configurations, 600 VDC system voltage, 2 to 25 kA bolted fault current, and up to a 152.4 mm (6 in) bus gap.

In [7] it was found that the HCB and VCB produced very similar incident energy values. In addition, the HCB and VCB configurations consistently produced incident energies higher than

the series open air. However, it should be noted that the open air to enclosure comparison in [7] did not have overlapping electrode configurations. Electrode configurations for a direct comparison to analyze the impact of the enclosure on incident energy for the VCB and HCB are the VOA and HOA configurations. Based on the findings of [17] and [18] the incident energy produced would likely still be higher for the enclosure than for the open air, but the same electrode configuration types should be used for quantifying the impact of the enclosure on incident energy.

The test results were analyzed to develop the equations (2-20) and (2-21) to determine incident energy exposure for 600 VDC systems. It was also found that the arc current was inversely proportional to the gap distance, and the incident energy was inversely proportional to the square of the working distance (in agreement with the findings in [10] for AC arc flash).

$$I_{arc} = 0.9063 * I_{bf}^{0.8927} - 0.1051 * e^{0.1093 * I_{bf}} * (G - 1) \qquad (2-20)$$

$$IE = (0.9694 * I_{arc} - 0.0589)(0.4793 * \ln(G) + 1.0027) * \left(\frac{t}{0.1}\right) * \left(\frac{6^2}{D^2}\right) \qquad (2-21)$$

Where,

I_{bf} bolted fault current (kA)

G gap distance (in)

D working distance (in)

t time (s)

IE incident energy (cal/cm^2)

The 125, and 260 VDC testing was used to modify Kinectric's existing ArcPro™ software [31] to estimate incident energy of DC arc flash hazards. The modified software was also used to

estimate the incident energy for the 600V DC tests. Its results were compared to the measured values of the 600 VDC tests. It was found that the ArcPro™ software [31] followed more closely with the actual results than Doan's method [20] (which was conservatively high the entire range with increasing disparity at higher fault currents). However, of the six data points shown in [7] at least three of the estimates were lower than the measured values. Therefore, it would not be recommended to use this software for 600 VDC systems. For 125 and 260 VDC [7] recommends using the ArcPro software to compute the incident energy, and (2-20) and (2-21) for 600 VDC systems with bolted fault currents between 2 and 25 kA, and gap distances up to 152.4 mm (6 in).

The DC arc flash testing performed by EPRI [8] was supplied DC power via PV arrays instead of a rectifier, as in [7]. The PV system was capable of 1000 kW power, and had an open circuit voltage of 1000 VDC. Seven tests were performed. Test parameters consisted of a VCB configuration, with an enclosure size of $508 \times 508 \times 508$ mm ($20 \times 20 \times 20$ in), 457.2 mm (18 in) working distance for ASTM 1959 calorimeters, 30 AWG copper pilot wire, 12.7 and 50.8 mm (0.5 and 2 in) bus gap, 125, 250, and 600 V, and nominal arc durations of 0.5, 2 and 10s. The power supplied and electrode spacing was varied during tests.

During testing the arc voltage and current waveforms were recorded. It was noted in [8] that the arc voltage had large fluctuations, especially at higher arc current, reaching up to 18 times the minimum value. They also noted that most of the electrical energy was converted into thermal, due to the minimal blast seen. As seen in Figure 7 the arc voltage and current values, at 12.7 mm (0.5 in) bus gap, were all on the constant-current region of the PV array I-V curve. Implying that for DC arc flashes of PV arrays, the arrays act as constant current sources, at almost the short circuit current of the array and above the maximum power point current, under the arc fault condition. It was also discovered that the arc current was independent of the bus gap, while the arc voltage inversely correlated with bus gap.

When compared to the leading DC arc flash incident energy estimation methods, (covered in Sections 2.2.1 and 2.2.2), Paukert's [32], Stokes and Oppenlander's [25], and Doan's [20] methods all deviated from the measured incident energy, as seen in Figure 7 and detailed in Table 1. Doan's was by far the most conservative, being around 3 to 10 times greater than the measured results. Meanwhile, Paukert's, and Stokes and Oppenlander's methods were generally conservative, but less than Doan, being slightly less than the measured results to 4 times higher than the measured results. The authors stress that additional testing is needed to better understand DC arc flash, and more accurately assess its risk. It is unfortunate that only seven tests were performed, but even the limited sample size highlights the disparity between the theoretical results and the measured results and the operation point of PV arrays under an arcing fault condition.

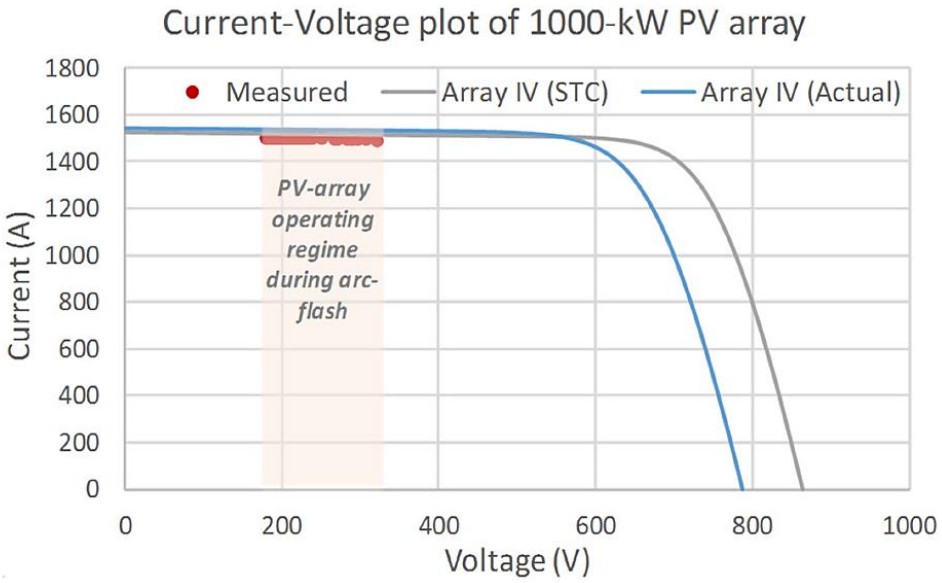

Figure 7 PV I-V Curve with Measured Arc Flash Data Points [8]

Table 1 Measured and Calculated Incident Energies [8]

Source size STC (Actual)	Gap (in)	Measured (cal/cm^2)	Paukert (cal/cm^2)	Stokes (cal/cm^2)	Doan (cal/cm^2)
125 (77)	2.0	0.8	3.09	3.38	8.29
250 (189)	0.5	0.1	0.21	0.22	0.52
500 (378)	0.5	1.4	1.15	1.36	5.10
500 (329)	0.5	0.6	0.99	1.17	4.41
1000 (881)	0.5	3.6	3.17	3.59	12.12
1000 (587)	2.0	2.1	3.69	3.76	7.88
1000 (690)	2.0	2.0	4.65	4.67	9.45

3.0 DC Arc Flash Experimental Testing

Increasing exposure to DC systems results in increased chances of personnel injury from DC electrical hazards, including arc flash. In 2018, IEEE Std 1584 – *IEEE Guide for Performing Arc-Flash Hazard Calculations*, [1], saw revisions that completely changed the standard based upon additional testing performed to address inadequacies in the original 2002 empirically derived model. However, this update did not include single phase AC or DC arc flash, thereby leaving NFPA 70E *Standard for Electrical Safety in the Workplace*, [6], to address DC arc flash electrical hazard. Unlike the equations developed in IEEE 1584 for three-phase AC systems, the equations in NFPA 70E are theoretical and were not supported with testing. Industry leading software tools for arc flash analysis, such as ETAP [9], develop their analysis techniques based on standards like IEEE 1584 and NFPA 70E.

As stated previously, DC arc flash testing and the results is limited in the public literature. The most notable testing was performed by Kinectrics [7] which found that the NFPA 70E/maximum power method was over-conservative. More recently, testing was performed by EPRI [8] with a PV power supply which found the NFPA 70E / maximum power method was about 3 to 10 times higher than their measured results.

Prior tests did not use vertical electrodes terminated in an insulating barrier inside a metal box / enclosure (VCBB) electrode configuration. As determined with AC testing and illustrated in [19], the VCBB configuration was deemed more applicable to real electrical equipment, saw increased incident energy and arcing current, decreased arc length, increased arc stabilization, and allowed for more arc sustainability for low voltage AC arc flash during testing when compared to the original vertical electrodes in a metal box / enclosure (VCB) configuration. The VCB

configuration was the initial electrode configuration used for arc testing in enclosures, and as illustrated in [17], [18], the VCB configuration yielded higher incident energy than open air due to the reflection of the energy by the enclosure out of the open front.

Reference [7] and [8] highlight the need for additional testing of DC arc flash to ensure that workers are adequately protected, but not unnecessarily over-burdened, with excessively over-conservative personal protective equipment (PPE). For this work, testing was performed at 130 VDC in an attempt to confirm the incident energy results obtained from NFPA 70E and ETAP, and to determine if there is a minimum available short circuit fault current where an arc flash event could no longer occur. For DC system evaluation, it was presumed that the benefits for increased energy results, and observable increases in low voltage sustainability in AC tests with the VCBB configuration would also be applicable for DC tests.

In Section 3.1, the experimental setup and testing procedures are detailed. In Section 3.2, the experimental results are presented. In Section 3.3, the theoretical models with the parameters of the experimental testing are used to calculate the estimated incident energy. Finally, in Section 3.4, the incident energies measured during testing are compared to the estimations from the theoretical models.

3.1 Experimental Set-Up and Test Procedure

As stated, the main purpose of performing our experiments is to determine for what system characteristics, if any, an arc is possible for DC based electrical systems. Testing was performed at 130 VDC with multiple fault currents, and bus gap distances. Bolted fault current varied from 1.893 kA to 27.5 kA, and bus gap distance varied from 12.7 mm (0.5 in) to 63.5 mm (2.5 in). The time constant of the system varied slightly with fault current due to the nature of the test circuit and ranged from 10.7 to 17.4 ms.

The test circuit, Figure 8, consists of a rectifier as the power supply, variable inductor (impedances changed based on the taps used) to set the time constant of the circuit, voltmeter, switch, ammeter, and the circuit under test. The rectifier was supplied by AC power through the lab's generators, Figure 9. The voltage after the inductor, but before the switch, is measured. Since the voltage is measured just before the unit under test, the arcing voltage V_{arc} could easily be obtained. The current is measured on the load side of the switch, before the unit under test to obtain the arcing current I_{arc}, as seen in Figure 8.

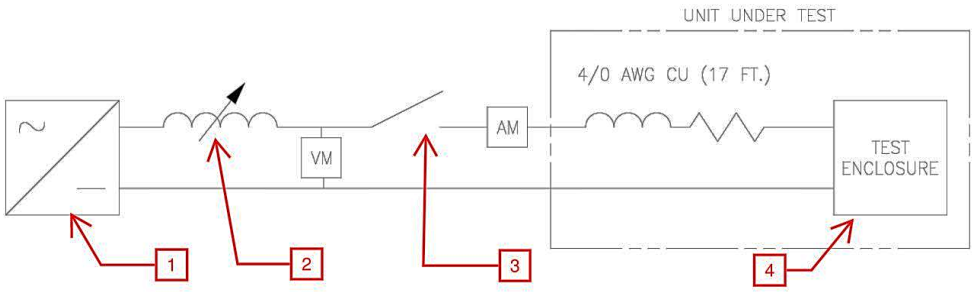

Figure 8 Simplified Test Circuit

Item 1: Rectifier, Item 2: Variable Indutor, Item 3: Switch, Item 4: Arc Flash Test Enclosure

Figure 9 Test Lab Generators

The circuit under test consists of cables from the lab's DC bus to the arc flash test enclosure. The arc flash test enclosure, Figure 10 and Figure 11, consists of copper bus bars, that are shorted together with a 14 AWG pilot wire, an insulating barrier that the bus bars sit into, and an insulating stand that holds the barrier up from the bottom of the enclosure. The pilot wire is used to initiate the short circuit fault current path. Due to the high levels of fault current, the small gauge wire melts like a fuse, and if the energy is sufficient enough to create and sustain the arc, an arc flash will occur. A longer time constant allows more energy to be transferred and therefore increases the probability of a sustainable arc flash. In front of the open-front enclosure, a calorimeter array, shown in Figure 10, is placed to measure the heat that is produced by a successful arc flash event.

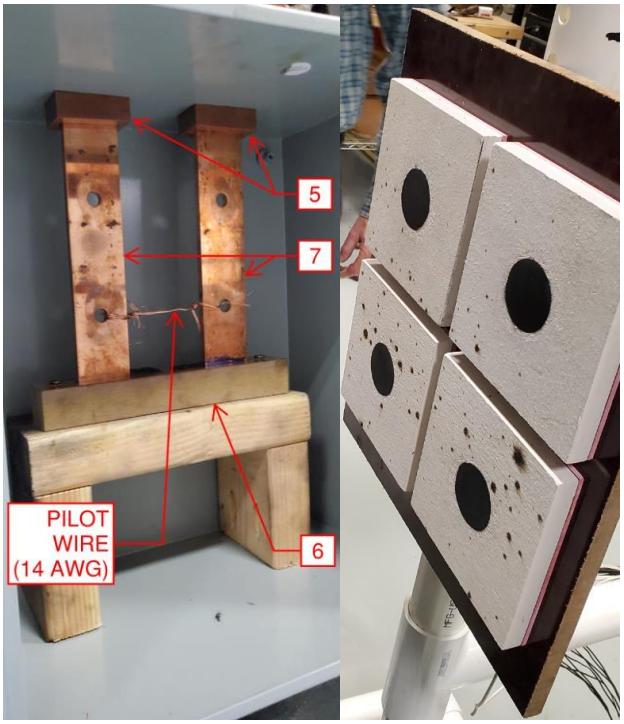

Figure 10 Arc Flash Test Enclosure (left), Monitor Sensors Calorimeter Array (right)

Item 5: Bus Entry Garolite Insulator Blocks, Item 6: Garolite Termination Insulator Block, Item 7: Bus Bars

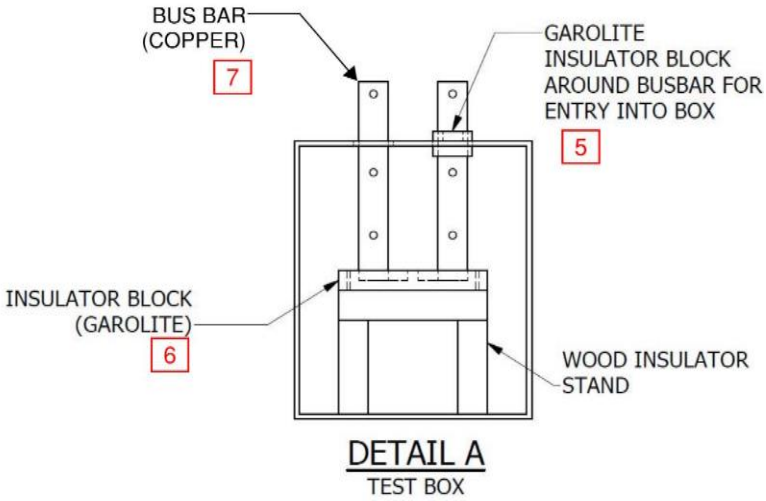

Figure 11 CAD Detail of Test Enclosure

3.1.1 Test Setup

More specifically, in Figure 12 and Figure 13, the circuit under test consists of 4/0 copper 2 kV RHW2 cable, about 4.57 m (15 ft) lengths, routed via one section of aluminum cable tray from the lab's DC bus to the mobile wall. The conductor passed through the mobile wall and terminated at the bus bars entering the enclosure, using mechanical lugs. The bus bars were rectangular copper bars, 6.35 mm (0.25 in) thick, 38.1 mm (1.5 in) wide, in a side-by-side configuration, as seen in Figure 10 and Figure 11. The bus bars were shorted during testing by bare 14 AWG stranded copper pilot wire. The distance from the back of the bus bars to the back of the enclosure was 47.625mm (1.875in).

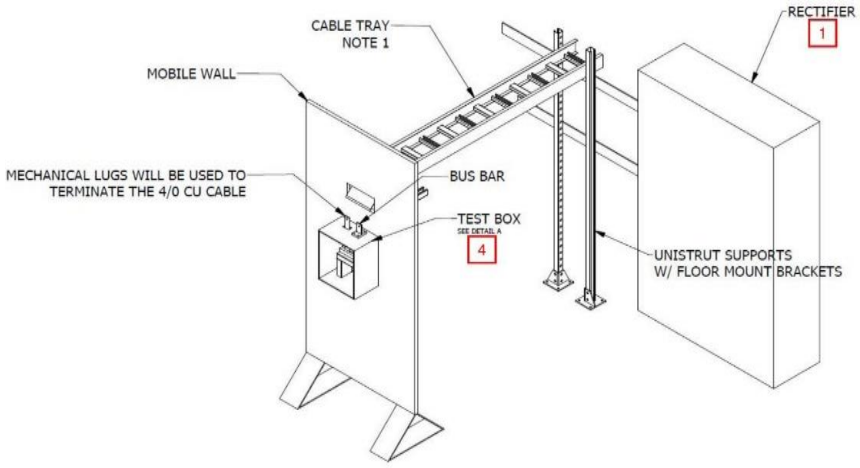

Figure 12 CAD Model of Test Setup

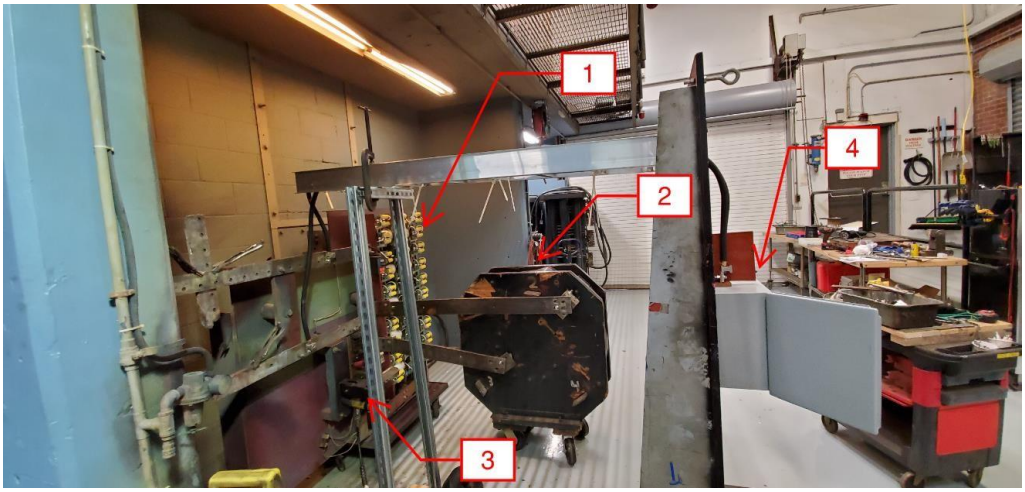

Figure 13 Testing Lab Test Setup

Insulating barriers made of Garolite were premade prior to testing. Two types of insulators were manufactured. One for the bus entry into the test enclosure, and the other was the termination insulating barrier as seen in Figure 10 and Figure 11. The termination insulating barrier was 38.1 mm (1.5 in) wide, 190.5 mm (7.5 in) long, and 25.4 mm (1 in) thick. The barrier had 6.35 mm (0.25 in) wide, 12.7 mm (0.5 in) deep, slots milled into the center to allow for the bus to set into the insulating block, creating the VCBB configuration, and still allowed for the gap distance to be varied. The insulating barrier was secured to the wooden insulating support, with the top of the insulator 158.75 mm (6.25 in) from the top of enclosure. The entry insulator was fashioned in a T-shape, allowing the bus to be insulated above and below the top of the enclosure.

There were five, 355.6 mm (14 in) × 304.8 mm (12 in) × 203.2 mm (8 in) enclosures with bus entries at the different bus gap spacing, listed in Table 2, in the top that accepted the Garolite entry insulators. The entry insulators were compression fit in the openings of the enclosure and did not require bolting onto the enclosure. The enclosures largely set the gap distance, while the slots of the insulating barrier allowed free movement between the different enclosures. 3M

Scotchfil insulating putty was used to fill the additional slot opening not filled by the copper bus bar. The putty is rated for 600 V and a temperature rating of 0 to 80 °C (32 to 176 °F).

Table 2 Testing Parameters

Factor	Levels
Gap Distance	12.7, 25.4, 38.1, 50.8, 63.5 mm (0.5, 0.75, 1.0, 1.5, 2.5 in)
System Voltage	130 VDC Stiff Source
Bolted Fault Current	1.893, 7.4, 12, 15.8, 20.9, 27.5 kA
L/R	10.7, 11.0, 11.1, 12.03, 13.47, 17.4 ms

Test Current must reach 99% of I_{SC} in five (5) time constants and sustain I_{SC} for 200 ms.

The four (4) calorimeter array, Figure 10, was mounted on a polyvinyl chloride (PVC) structure. The PVC structure was then secured to the mobile wall such that the calorimeter array was 457.2 mm (18 in) from the bus bars. This value will be referred to as the working distance, which is the distance from the arc to a worker's head/chest. The PVC structure was adjustable to allow the top row of calorimeters to be centered at approximately the top of the insulating barrier. Based on the AC testing of the VCBB configuration in [19], if an arc was sustainable, it was believed that it would also occur just above the insulating barrier. Therefore, it was desirable to have a calorimeter centered on this elevation to capture the heat from the arc flash event. The calorimeters were manufactured according to ASTM F1959 standard [33], as a monitor sensor. The calorimeters consist of a copper disk, thermocouple, and sensor holder. The copper disks are 18 g, 101 grade copper, 40 mm diameter, 1.6 mm thick, and have a high-temperature flat black coating with an absorptivity of 0.9 or greater. The thermocouples are 30 AWG, type K

thermocouples. The sensor holder is 127 mm (5 in) x 127 mm (5 in) and 12.7 mm (0.5 in) thick made from insulation board that has a density of 737 kg/m^3 (46 lbs/ft^3), and thermal conductivity of 12 W/m·K per ASTM C 177. The insulation board is backed by a 3.175 mm (1/8") thick Arc-Resistant GPO3 fiberglass sheet, to secure the wire, and was adhered to the insulation board with high-temperature (343 °C) silicon adhesive.

The thermocouples were terminated to extension wires that entered the control room. The thermocouples were terminated on the data acquisition device (DAQ). The DAQ was an 8-channel USB powered Data Translation DT9828. The module came with its own Omni Software for drivers, and a data logging application QuickDAQ, which was used to capture the temperature readings. The DAQ sampled the temperature readings at 150 Hz for all four thermocouples simultaneously.

To summarize, the overall test setup can be seen in Figure 12 and Figure 13, and the physical parameters, as detailed above are summarized in Table 3. Testing factors, gap distance, system voltage, bolted fault current, and L/R ratio, and levels, varying values of the factors, were based on a 125 VDC battery supplied control system in an electric generating facility. The factors and their corresponding levels are detailed in Table 2.

Table 3 Test Setup Physical Parameters and Dimensions

Test Material	Details
Enclosure Size	355.6 × 304.8 × 203.2 mm (14 × 12 × 8 in)
Electrode Configuration	VCBB
Bus Bars	6.35 mm thick, 76.2 mm wide (0.25 in thick, 1.5 in wide)
Insulating Barrier	38.1 × 190.5 × 25.4 mm (1.5 × 7.5 × 1 in)
Working Distance	457.2 mm (18 in)
Pilot Wire	14 AWG

The enclosure size, gap distance, and working distance were all based on the IEEE 1584 for panelboards. The electrode configuration was chosen based on the 2018 edition of IEEE 1584; typical DC control system equipment, and the configuration that would yield the highest incident energy. The VCBB configuration is applicable to battery chargers and distribution panelboards, since the conductors are terminating into terminals for the overcurrent protective device, and other equipment where the conductors enter a terminal block.

The system voltage was selected based on the desire to test 125 VDC systems; however, it was common to see battery chargers output 130 VDC, and subsequently the battery banks. Therefore, it seemed prudent to test at this higher DC voltage.

The available bolted fault current for the testing was based on a lead acid battery bank short circuit capabilities. The range was based on the minimum (0.47 kA) and maximum (27 kA) of the entire lineup of a manufacturer's line of Valve-Regulated Lead-Acid (VRLA) and Vented Lead-Acid (VLA) batteries currently installed at the subject generating station.

The L/R ratios were determined using suggestions from [23], which presented common time constants for different systems/equipment types. Reference [23] stated that for control

systems the time constants were 10 ms or less, while UPS and battery systems tended to be lower, usually less than 5 ms. The 10 ms time constant was chosen as the nominal value, since a larger time constant allows for more energy to be transferred.

The working distance was set based on IEEE 1584 where the typical working distance was 18 inches for panelboards, junction boxes, MCCs, and other equipment. This also encompasses the large majority of DC equipment. The standard's minimum testing distance is 12 inches, since any closer would put the worker in the contact with the arc blast (arc cloud and plasma), however, that is not a defined typical working distance for electrical equipment, and therefore was not included.

The minimum gap distance of 12.7 mm (0.5 in) was based on the minimum allowable spacing between conductors of opposite polarity up to 125 V for switchboards per UL 891 [34].

3.1.2 Test Procedure

The testing performed was a sensitivity analysis with respect to the fault current and gap distance. In general, the tests were performed such that the bus gap distance was increased or decreased at each fault current level depending upon the sustainability of the arc. For an un-sustained test, the gap distance was decreased, and for a sustained test, the gap distance was increased. Once testing was performed at each bus gap, as needed, the bolted fault current was increased or decreased based on the arc's sustainability. If at any gap distance the arc flash event was sustainable, the bolted fault current was decreased. If the bolted fault current was not sustainable at any bus gap distance, then the bolted fault current was increased within the bolted fault current range listed in Table 2.

At each new bolted fault current, a calibration test, where the arc flash enclosure bus bars are shorted with an additional bus bar was performed at the new fault current to ensure that the desired L/R ratio and bolted fault current was reached. The calibration tests were repeated as needed to reach the desired L/R ratio and bolted fault current.

Testing started at the middle of the bolted fault current range listed in Table 2, at 12 kA with an L/R ratio of 10.7 ms. The testing was started in the middle in order to decrease the number of iterations required when trying to find if there was a minimum fault current for arc flash occurrence. If at 12 kA and any gap distance in the range, the test always sustained then no further testing above 12 kA is required. If it never sustained, then testing would not be required below 12 kA.

The fault current was increased/decreased at intervals of approximately 5 kA until the fault current level was about 2 kA, or the maximum fault current, 27 kA, was reached. See Table 2 for the fault current levels and corresponding L/R ratios used during testing.

In the event that an arc flash event did not occur, the test was repeated at least one additional time to ensure the arc flash event still did not occur. If an event occurred after the first re-test, no additional tests were required for sustainability, and the standard testing process was resumed. In the event that an arc flash still did not occur on a retest, the gap distance was decreased by about 12.7 mm (0.5 in) increments, to the values listed in Table 2 and performed at the same fault current.

After each failed test, the insulating barrier was cleaned using a wire brush and wiped clean with a shop towel. The insulating putty was replaced as needed. The 3M putty was flammable and sometimes caught fire, typically only on a successful arc flash event. The pilot wire was replaced and then the test was repeated.

On a repeated test with a failure, the test box was replaced with the next smaller gap distance, and the insulating barrier and bus bars were cleaned before testing.

On a successful arc flash event, the test box was replaced with the next larger gap distance. The insulating barrier was generally replaced, due to damage sustained from the arc flash event. Insulators that were salvageable were cleaned using a wire brush and shop towel. After cleaning they were ohmed to ensure that the insulating barrier was still acceptable and not impregnated with electrode material from the arc flash event. The bus bars were eroded during testing, as seen in Figure 14, and were replaced or flipped after a successful test to keep a flat edge at the bus gap. Bus bars that were salvageable to be flipped, were cleaned with wire brush, file, and abrasive pads, as needed. Excess copper that melted and prevented the bus bar from fitting in the insulating barrier slot, was removed to obtain the full depth of the insulator.

Figure 14 Bus Bar Erosion

3.2 Test Results

A list of tests with the fault current, gap distance, time constant, and outcome is shown in Table 4. In Table 4 test numbers 1, 12, 14, 16, 23, and 27 are not shown since they were calibration tests only. A table indicating the outcome of the sustainability, incident energy, and the test parameters is shown in Table 5. Note that only one test resulted in an incident energy over 1.2 cal/cm^2.

Table 4 Testing Outcomes

Test No.	Bus Gap (mm) [in]	I_{bf} (kA)	Time Constant (ms)	Test Result
2	12.7 [0.5]	12	10.7	Sustained
3, 4, 5	63.5 [2.5]	12	10.7	Un-sustained
6, 7, 8	38.1 [1.5]	12	10.7	Un-sustained
9, 10, 11	25.4 [1]	12	10.7	Un-sustained
13	12.7 [0.5]	7.4	11.1	Sustained
15	12.7 [0.5]	1.893	12.03	Sustained
17, 18, 19	38.1 [1.5]	20.9	13.47	Un-sustained
20	25.4 [1]	20.9	13.47	Un-sustained
21	25.4 [1]	20.9	13.47	Sustained
22	25.4 [1]	20.9	13.47	Sustained
24	19.05 [0.75]	15.8	11	Sustained
25	25.4 [1]	15.8	11	Un-sustained
26	25.4 [1]	15.8	11	Sustained
28	25.4 [1]	27.5	17.4	Un-sustained
29	25.4 [1]	27.5	17.4	Sustained
30	12.7 [0.5]	27.5	17.4	Sustained
31	38.1 [1.5]	27.5	17.4	Un-sustained

Missing test numbers are calibration tests which are not included.

Table 5 Test Results Summary

I_{bf} (kA)	Bus Gap (mm) [in]					Time Constant (ms)
	12.7 [0.5]	19.05 [0.75]	25.4 [1]	38.1 [1.5]	63.5 [2.5]	
1.893	0.52*	**				12.03
7.4	0.67*	**				11.1
12	0.80*		*	*	*	10.7
15.8		0.72*	0.66*			11.0
20.9			0.85, 0.70*	*	**	13.47
27.5	1.87*		0.97*	*	**	17.4

I_{bf} = Bolted Fault Current

#* = Incident Energy (cal/cm2) Measured, Actual Test

** = Predicted Result

Green Shading Indicates Sustained

Red Shading Indicates Un-sustained

The copper bus bars experienced significant erosion for tests that were sustainable. Bus bar erosions measured over 12.7 mm (0.5 in). Test 30 had the highest erosion with bus bar erosion measuring approximately 15.875 mm (5/8 in), as seen in Figure 14.

3.2.1 Arc Flash Sustainability

Table 4 and Table 5 show that arc flash events were sustainable through the entire available fault current range tested. In [1], the authors state, “Sustainable arcs are possible but less likely in three-phase systems operating at 240 V nominal or less with an available short-circuit current less than 2000 A.” Hence, it was expected that a minimum fault current would be discovered where it would not be possible to have a sustainable arc flash event. However, such a conclusion could not

be made for 125/130 V DC systems. If the 125 V DC equipment is limited to a minimum of a 25.4 mm (1 in) bus gap, then a similar statement could be made for 125/130 V DC systems. As seen in the testing at 12 kA, it was not possible to sustain an arc flash event at the 25.4 mm (1 in) bus gap on three separate trials.

It is interesting to note that no arc flash event was sustainable beyond the 25.4 mm (1 in) gap. Even at the maximum fault current tested at 27.5 kA, the 38.1 mm (1.5 in) gap was not sustainable. It self-extinguished rapidly, ending approximately 45 ms after the pilot wire was melted as seen in Figure 15. This was at least twice as long as the other non-sustaining 38.1 mm (1.5 in) gap tests.

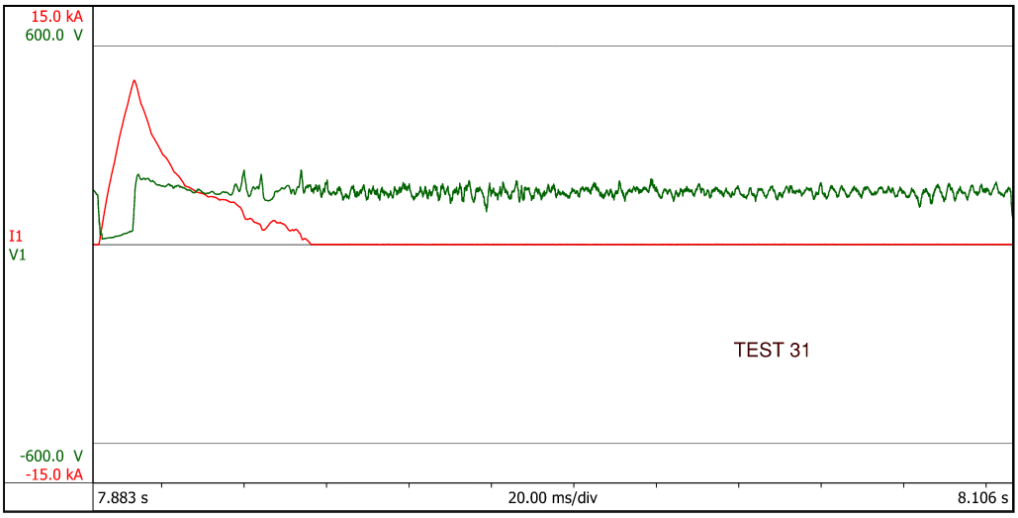

Figure 15 Test 31 Current and Voltage Waveforms

Un-sustained arc flash event, fault current (red) and voltage (green) waveforms. 38.1 mm (1.5 in) gap distance, 17.4 ms time constant, and 27.5 kA bolted fault current.

3.2.2 Gap Distance Impact on Incident Energy Levels

As seen by the un-sustainability of an arc flash event at gap distances beyond the 25.4 mm (1 in) bus gap, it is clear that gap distance has a large impact on sustainability. In addition, gap distance also has a large impact on the incident energy. It was found that incident energy was inversely proportional to the gap distance. As seen in

Table 5, the incident energy of a 12.7 mm (0.5 in) gap at 12 kA was 0.80 cal/cm^2. While the incident energy of a 19.05 mm (0.75 in) gap at 15.8 kA had a lower incident energy of 0.72 cal/cm^2. Increasing the gap distance by only 6.35 mm (0.25 in) caused the incident energy to be lower even with an additional 3.8 kA available fault current. Two other examples showing the impact of gap distance are the tests occurring at 15.8 kA and 27.5 kA. At 15.8 kA bolted fault current, the bus gap was increased by 33% (19.05 mm (0.75 in) to 25.4 mm (1 in)) causing an 8% decrease in the incident energy (0.72 to 0.66 cal/cm^2). At 27.5 kA bolted fault current, the bus gap increased by 100% (12.7 mm (0.5 in) to 25.4 mm (1 in)) causing a 48% decrease in the incident energy (1.87 to 0.97 cal/cm^2).

3.2.3 Peak Fault Current Impacts on Sustained Arcs

In three instances an arc flash event sustained on the second trial of a test after it did not sustain on the first trial, all of which were at a 25.4 mm (1 in) bus gap. For test 20 the arc did not sustain, as seen in Figure 16. However, the next test with the same parameters, test 21, the arc did sustain with fault current initially falling steadily after the pilot wire melted before flattening out around 2.2 kA at about 170 ms into the test, as seen in Figure 17. Since this was the first experience when an arc flash event occurred after an un-sustaining event, the same conditions were re-

evaluated. In test 22, an arc flash event occurred, however, it self-extinguished around 160 ms after the pilot wire melted, as seen in Figure 18. In comparison to test 21 in Figure 17, they both decrease steadily after the pilot wire melts. However, in test 21 the current flattens out at around 125 ms after the pilot wire melts while for test 22 the current exponentially decays. At about 152 ms, after the pilot wire melts, the current collapses and is extinguished at about 159 ms, after the pilot wire melts.

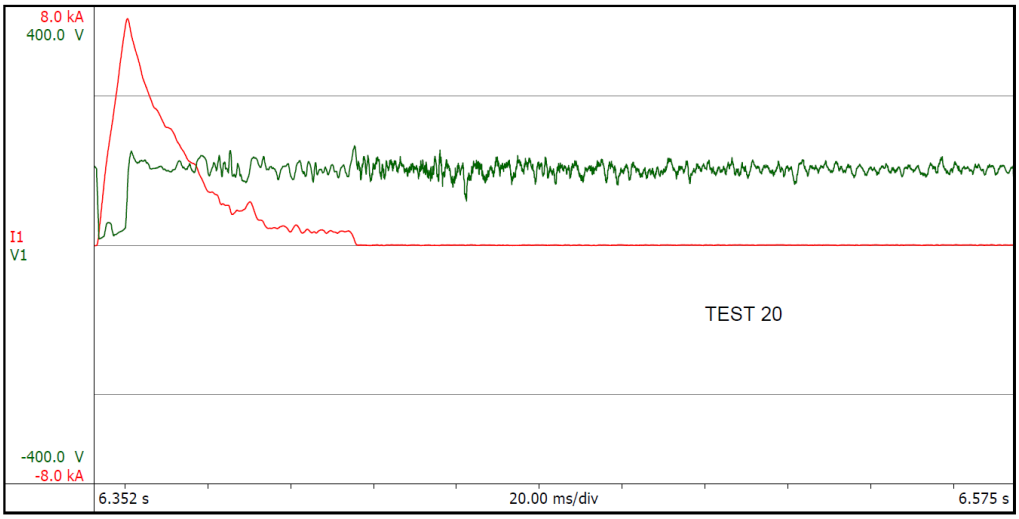

Figure 16 Test 20 Current and Voltage Waveforms

Un-sustained arc flash event, fault current (red) and voltage (green) waveforms. 25.4 mm (1 in) gap distance, 13.47 ms time constant, and 20.9 kA bolted fault current.

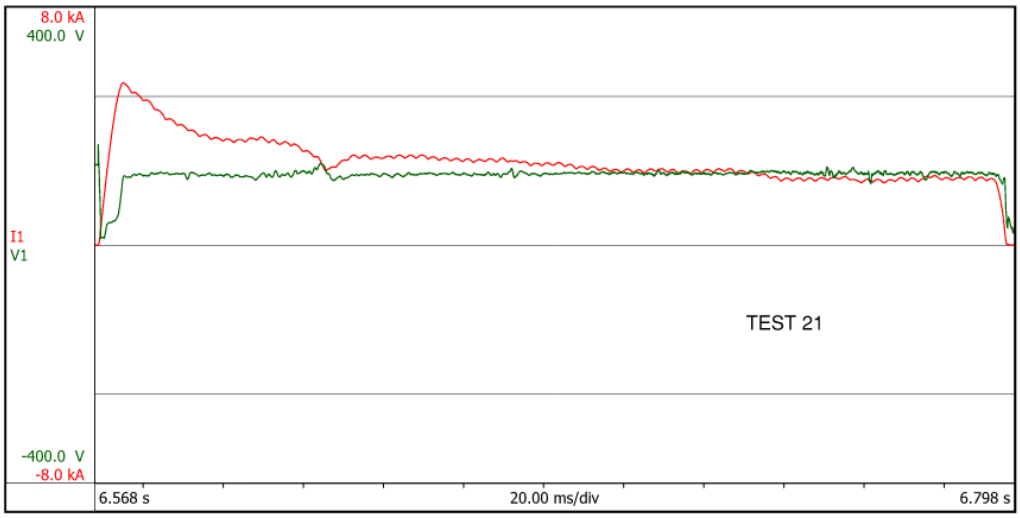

Figure 17 Test 21 Current and Voltage Waveforms

Sustained arc flash event, fault current (red) and voltage (green) waveforms. 25.4 mm (1 in) gap distance, 13.47 ms time constant, and 20.9 kA bolted fault current.

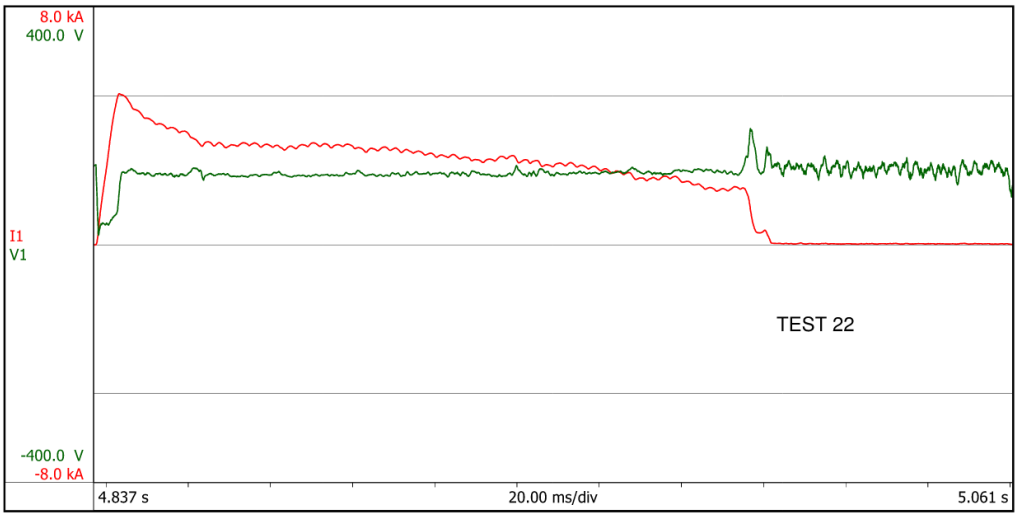

Figure 18 Test 22 Current and Voltage Waveforms

Self-extinguishing sustainable arc flash event, fault current (red) and voltage (green) waveforms. 25.4 mm (1 in) gap distance, 13.47 ms time constant, and 20.9 kA bolted fault current.

One contributing factor to the difference between the results of test 21 and 22 is the peak current. The current peaked at 5.455 kA for test 21 while the current only peaked at 5.078 kA for test 22. Both of these tests had current peaks that were relatively close, unlike the un-sustaining event that had a current peak of 7.6 kA. The experiments show that at a much higher peak current, 7.6 kA, the arc did not sustain while at a lower current, 5.455 kA, the arc did. However, the slightly lower current, 5.078 kA, did not sustain the entire duration.

To further explore the coupling between peak fault current and arc sustainability, a few additional tests were run to gather additional observations. Tests 25 and 26 utilized a 25.4 mm (1 in) bus gap, and a *bolted fault current of 15.8 kA*. Test 25, Figure 19, did not sustain, while the retest, test 26 in Figure 20, did.

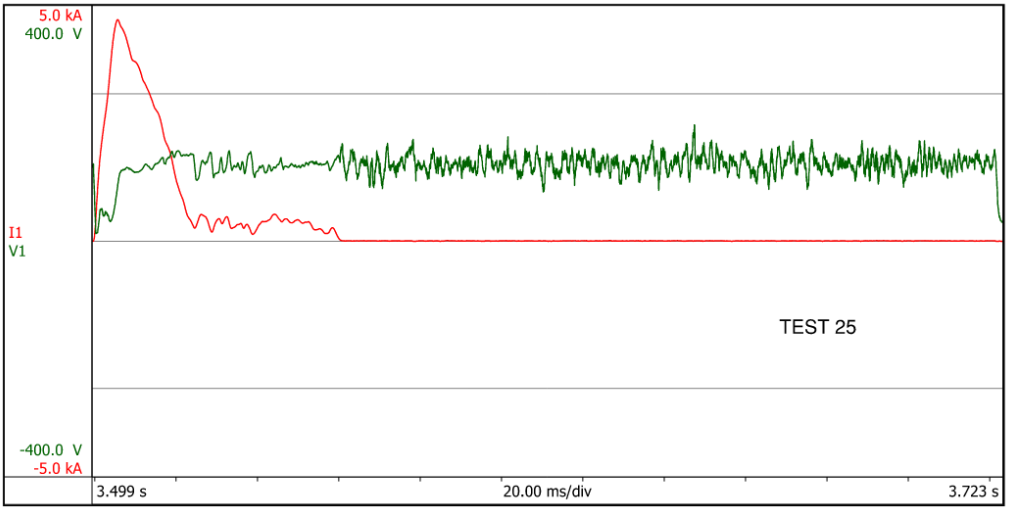

Figure 19 Test 25 Current and Voltage Waveforms

Un-sustained arc flash event, fault current (red) and voltage (green) waveforms. 25.4 mm (1 in) gap distance, 11 ms time constant, and 15.8 kA bolted fault current.

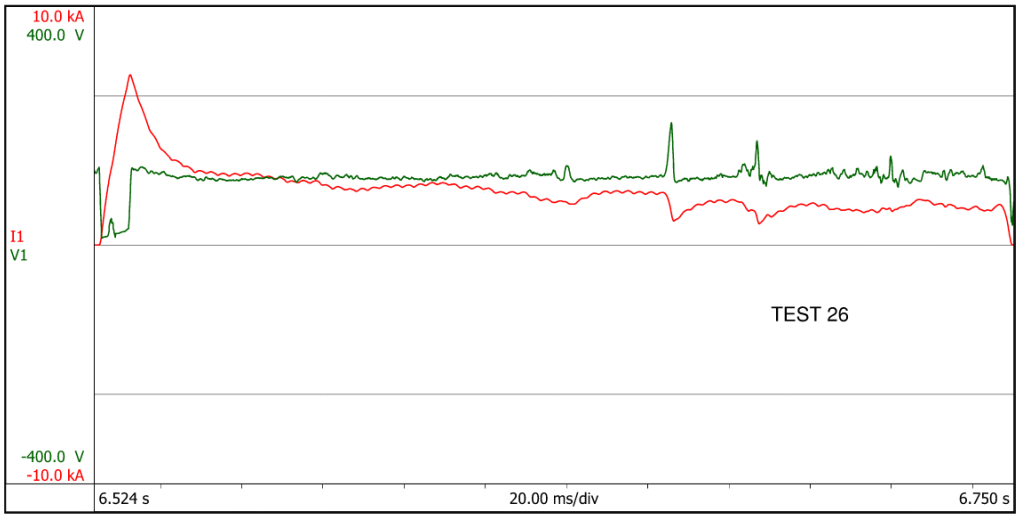

Figure 20 Test 26 Current and Voltage Waveforms

Sustained arc flash event, fault current (red) and voltage (green) waveforms. 25.4 mm (1 in) gap distance, 11 ms time constant, and 15.8 kA bolted fault current.

For test 25, the peak current reached 4.698 kA, at which point the pilot wire melted. After melting, the current decreased rapidly, dropping to about 280 A in 19 ms, and the current reached zero 55 ms after the pilot wire melted.

For test 26, the arc sustained with the fault current decreasing rapidly after the pilot wire melts, as typically seen, and flattening out around 2.5 kA. Additionally, at about 134 ms and 155 ms after the pilot wire melts, the current sharply decreases as if about to extinguish, similar to what is seen in test 22, however, in this test case the current recovers both times and sustains the arc.

Tests 28 and 29 utilized a 25.4 mm (1 in) bus gap, and a *bolted fault current of 27.5 kA*. Test 28, Figure 21, did not sustain, while the retest, test 29 in Figure 22, did. On test 28 the peak current reached 6.21 kA, at which point the pilot wire melted. After melting, the current decreased very rapidly, dropping to about zero in about 3.1 ms.

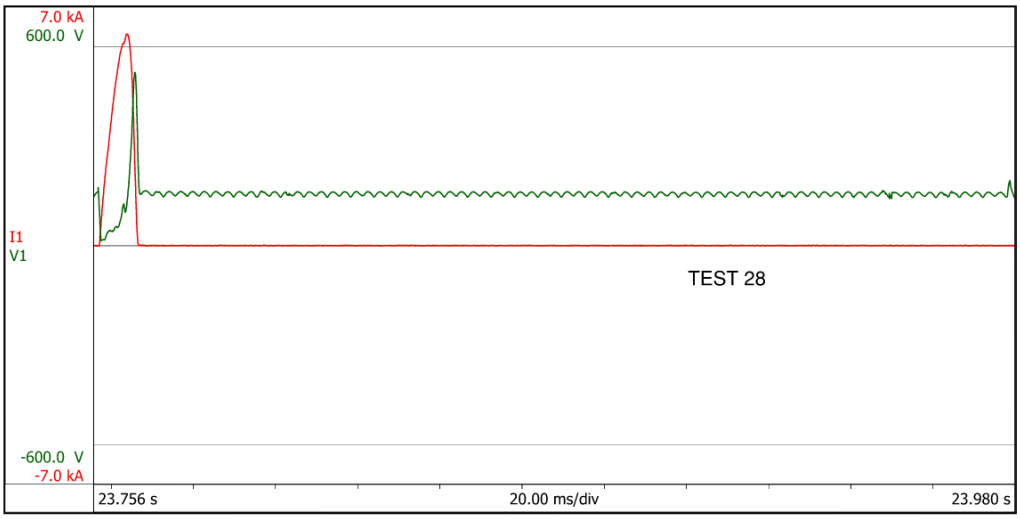

Figure 21 Test 28 Current and Voltage Waveforms

Un-sustained arc flash event, fault current (red) and voltage (green) waveforms. 25.4 mm (1 in) gap distance, 17.4 ms time constant, and 27.5 kA bolted fault current.

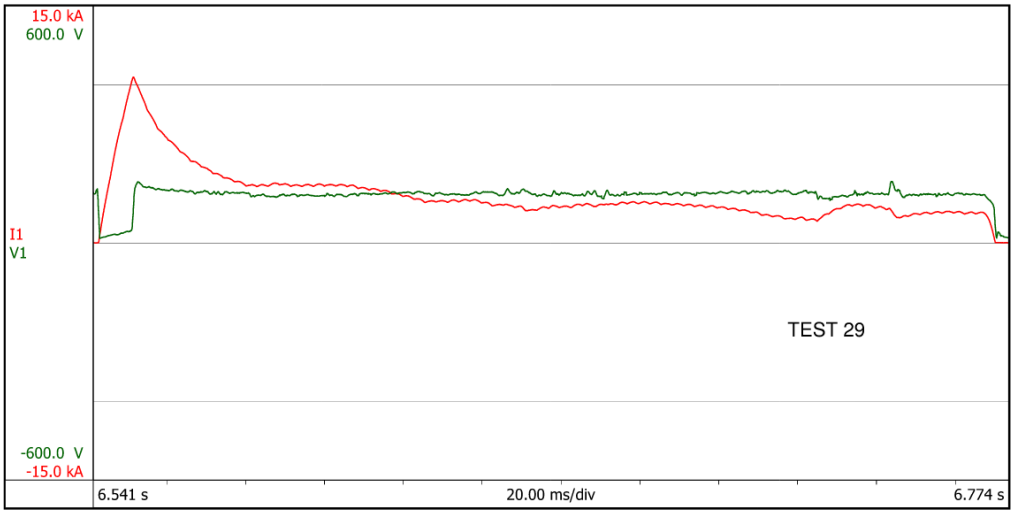

Figure 22 Test 29 Current and Voltage Waveforms

Sustained arc flash event, fault current (red) and voltage (green) waveforms. 25.4 mm (1 in) gap distance, 17.4 ms time constant, and 27.5 kA bolted fault current.

Test 29 sustained with the fault current decreasing rapidly after the pilot wire melts and flattening out to around 3.6 kA in about 29 ms. After the pilot wire melts, the current settles to 2.5 kA after 130 ms have passed. Additionally, at about 175 ms and 195 ms after the pilot wire melts, the current decreases as if it were to extinguish, similar to what has been seen in test 26. However, in this test case, the current did not decrease as rapidly as seen in test 26.

Observing these three testing groups the largest difference between each set of tests is the peak current. For tests 20 through 22, the peak currents were 7.6 kA, 5.46 kA, and 5.08 kA respectively. Unsurprisingly, the higher peak current resulted from the time it took for the pilot wire to melt. The result that is surprising is that the highest peak current was the test that was unable to sustain, while the other two tests had lower currents and were able to sustain for most, or all, of the test. In addition, the peak current of test 22 was only about 380 A less than test 21, however, test 21 was able to sustain the entire test duration of 200 ms, while the slightly lower test 22 did not. For tests 25 and 26, the opposite occurred. Tests 25 and 26 had peak currents of 4.7 kA, and 7.13 kA respectively. In this case the higher peak current was able to sustain, while the lower was not. Tests 28 and 29 had peak currents of 6.21 kA and 10.5 kA respectively. Again the higher peak current (longer time taken for the pilot wire to melt) test sustained while the lower peak current did not.

As stated earlier, all three of these tests groups had the second test sustain while the first was un-sustained. This can be attributed to excess carbon and copper that remained after the first test. Although the insulating barrier, and bars, were cleaned between tests, not all products from the arc can be removed by normal means. Having the excess conductive material during the test would make the arc more likely to sustain. This presence of conductive material within the equipment, however, would be more representative of typical industrial installations. Electrical

equipment, especially in steel mills, power plants and other heavy industrial facilities, would not be in pristine condition even after a maintenance outage. Since access to bars, terminals and other current carrying parts within the gear is virtually impossible to clean to the level in the lab, the existence of conductive dusts and materials in the switchgear presents an increased likelihood of a sustained arc when a fault has occurred.

The complete set of current and voltage waveforms captured from the thirty-one (31) tests are included in Appendix A.

3.3 Incident Energy Results Based on Theoretical Equations

Theoretical models were created/utilized to compare with the experimental results. The theoretical models used were the NFPA 70E – 2015 [22], NFPA 70E – 2018 [6], and maximum power, Stokes and Oppenlander, and Paukert methods using ETAP 19.5.0. There are additional theoretical models as summarized in [14], but these five methods are the focus for the comparative analysis.

The NFPA 70E, Standard for Electrical Safety in the Workplace, establishes requirements and guidelines to address the safety of employees exposed to electrical hazards, in particular interacting with energized equipment, in order to create a safe environment for employees either performing maintenance or general workplace electrical safety practices. In article 130.5 of NFPA 70E – 2018, addressing arc flash risk assessment, if the use of PPE is deemed necessary after a risk assessment, the NFPA 70E – 2018 allows for the use of one of the two different methods of determining appropriate PPE for workers, but not both. Either the incident energy analysis method or the arc flash PPE category method can be used as per Article 130.5(F).

The incident energy analysis method takes into consideration the working distance, the overcurrent protective device, equipment condition, and fault clearing time (as per Article 130.5(G)), and the PPE is selected using Table 130.5(G), which is split into two incident energy exposure categories (1.2 to 12 cal/cm^2 and greater than 12 cal/cm^2). Informative Annex D has information regarding the calculation of both AC and DC incident energy calculations. DC incident energy calculation methods are detailed in Section D.5. Section D.5.1 is based on the maximum power method developed by Doan [20], and applies to DC systems up to 1000V. Doan estimated the maximum power of the arc by having the arcing resistance equal to the system resistance and then developed an equation of the incident energy based on the clearing time and working distance. This approach is very similar to the method developed by Lee for AC systems [10], which was also based on the maximum power of an arc based on the available short circuit current, to find the maximum theoretical model of radiant heating from an arcing fault. Per Section D.5.1, the arcing current is calculated with (3-1) and used to calculate the incident energy, (3-2).

$$I_{arc} = 0.5 \times I_{bf} \qquad (3-1)$$

$$IE_m = 0.01 \times V_{sys} \times I_{arc} \times T_{arc}/D^2 \qquad (3-2)$$

Where,

I_{arc} = arcing current (A)

I_{bf} = system bolted fault current (A)

IE_m = estimated DC arc flash incident energy at the maximum power point (cal/cm^2)

V_{sys} = system voltage (V)

T_{arc} = arcing time (s)

D = working distance (cm)

If the arc is in a box, or enclosure, the standard recommends to consider PPE that is beyond the requirements of the PPE category method. This is different than the previous recommendation of multiplying the result of (3-2) by a factor of three in the 2015 edition for arcs in an enclosure. A bias or factor does seem prudent to add, based on the findings in [17] and [18] for AC arc flash testing.

The maximum power method is also recommended by the National Electrical Safety Code [21], which provides guidelines to protect workers and facilities of utilities, thereby solidifying Doan's method to be the most accepted method in industry for calculating incident energy for DC arc flash. However, there are many sources, [26][27]-[29] that have illustrated the differences between PV systems and other DC systems, namely its non-linear I-V characteristic, and the close proximity of the short circuit current and normal operating point. Most of the references state that the typical maximum power transfer method developed by Doan is not applicable to PV systems. PV system arc flash testing has been performed, and in [8] concluded that no theoretical model adequately quantifies the incident energy.

The PPE category method, Article 130.7(C)(15), is applicable for AC and DC systems of specified parameters, such as voltage, available fault current, equipment type, working distance,

and arc duration. If the parameters are outside of those specified, this method cannot be used and the incident energy calculation method must be used. For DC systems, Table 130.7(C)(15)(b) is used. The PPE category tables (task tables) classify PPE into four categories (Category 1 through 4) corresponding to arc clothing ratings of 4 cal/cm^2, 8 cal/cm^2, 25 cal/cm^2, and 40 cal/cm^2 respectively, and additional necessary ancillary equipment such as hard hats, hearing protection, leather gloves, etc. which also vary based on the level of incident energy.

In the testing performed, only the tests that were below 15 kA bolted fault current are applicable to use the PPE category method.

The results of (3-2), the 2015 factor of 3 method, and the 2018 method for arcs in an enclosure for each test method are listed in Table 6. The working distance for all tests were 45.72 cm (18 in), the system voltage was 130 V, and the arcing time was 200 ms. It is important to note that none of these methods consider bus gap distance as a factor in determining incident energy, but this was seen as an important variable from our experimental trials. It is easy to see from Table 6 that the PPE requirements when selecting PPE from the task tables is much higher than the previous recommendation of multiplying the incident energy result from (3-2) by three for arcs in an enclosure.

Table 6 NFPA 70E – 2015 and 2018 Methods

I_{bf} (kA)	I_{arc} (kA)	IE_m (cal/cm^2)	NFPA 70E – 2015 IE Rating (cal/cm^2)	NFPA 70E – 2018 IE Rating (cal/cm^2)
1.893	0.9465	0.12	0.35	8
7.4	3.7	0.46	1.38	25
12	6	0.75	2.24	25
15.8	7.9	0.98	2.95	N/A
20.9	10.45	1.30	3.90	N/A
27.5	13.75	1.71	5.13	N/A

I_{arc} = Arcing Current

IE_m = Incident Energy at Maximum Power Point from (3-2)

IE = Incident Energy

NFPA 70E – 2015 is with the factor of three for enclosures

NFPA 70E – 2018 are the values specified by the task tables to be used for arcs in an enclosure. Values marked N/A exceed the parameters for the task tables and therefore the tables cannot be used.

As systems get more complex these calculations become more cumbersome, and therefore power system analysis software is utilized for arc flash analysis/studies. The majority of arc flash studies performed in industry are done using various power system analysis software capable of arc flash analysis such as, ETAP, SKM, EasyPower, etc. ETAP 19.5.0 was used to model the experimental test setup and parameters and obtain arc flash incident energy values using ETAP's available arc flash calculation methods. ETAP has three different DC arc flash methods; maximum power, Paukert, and Stokes and Oppenlander. Paukert's [32], and Stokes and Oppenlander's [25] methods are based on arc resistance. Their findings and a comparison of their results is detailed in [24]. It was concluded that their models generally agreed with each other; however, they did have some deviation especially for larger gap distances. The one-line diagram from ETAP is shown in Figure 23.

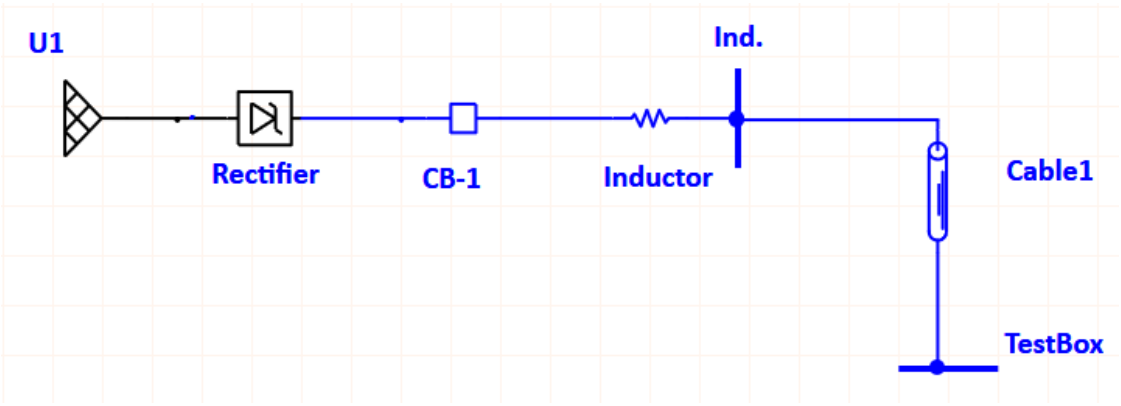

Figure 23 ETAP 19.5.0 One-Line Diagram of Test Circuit

The TestBox bus, is modeled as the test enclosure mounted on the mobile wall. The settings of the box were changed to match those of the test enclosure, such as the equipment properties, and conductor/electrode properties. The settings input were: equipment type as panelboard, box was checked, the test setup enclosure dimensions were input, reflectivity coefficients were left at the default values, the gap between conductors was set at the minimum values used during testing at each fault current level, 12.7 mm (0.5 in), 19.05 mm (0.75 in), and 25.4 mm (1 in), conductor orientation was set to vertical, the termination was set to insulating barrier, and the conductor type was set to copper. Cable1 is modeled as the 4.57 m (15 ft) 4/0 copper cable that was routed via cable tray from the DC bus to the test enclosure.

The test circuit inductor was modeled as a DC impedance with resistance and inductance values to obtain the L/R ratio for each test setup. Since the experimental test setup had a protective device for disconnecting power after 200 ms to the test circuit on the AC side it was necessary to add a DC circuit breaker CB-1 to the circuit. A DC circuit breaker without an instantaneous setting and a short-time pickup long enough to not trip in 200 ms was selected. The arc flash study fault

clearing time setting was changed to limit the maximum fault clearing time to 200 ms. Alternatively, the protective device could be excluded if the TestBox bus, arc flash user-defined source protective device, setting was changed to use a fixed fault clearing time. Lastly, the rectifier was modeled to provide the bolted fault current for each test setup, by varying the short circuit contribution.

The analyses were run for each test scenario with all three of the different arc flash methods available by ETAP 19.5.0. The results are listed in Table 7.

Table 7 ETAP 19.5.0 Arc Flash Results

I_{bf} (kA)	Maximum Power (cal/cm^2)	Paukert (cal/cm^2)	Stokes & Oppenlander (cal/cm^2)
1.893	0.353	0.164	0.17
7.4	1.381	0.666	0.66
12	2.239	1.078	1.055
15.8	2.948	1.074	1.292
20.9	3.901	1.323	1.502
27.5	5.131	2.401	2.316

3.4 Comparison of Industry Theoretical Models with Experimental Results

3.4.1 Incident Energy Comparison of NFPA 70E and Experimental Results

The testing data was compared to the results obtained from the NFPA 70E methods, as consolidated in Table 8.

Table 8 Test Results and NFPA 70E – 2015 and 2018 Methods

I_{bf} (kA)	IE Measured (cal/cm^2)	IE_m (cal/cm^2)	NFPA 70E – 2015 IE Rating (cal/cm^2)	NFPA 70E – 2018 IE Rating (cal/cm^2)
1.893	0.52	0.12	0.35	8
7.4	0.67	0.46	1.38	25
12	0.8	0.75	2.24	25
15.8	0.72	0.98	2.95	N/A
20.9	0.85	1.30	3.90	N/A
27.5	1.87	1.71	5.13	N/A

IE Measured = Maximum Incident Energy Measured During Testing (at fault current level)

NFPA 70E – 2015 is with the factor of three for enclosures

NFPA 70E – 2018 are the values specified by the task tables to be used for arcs in an enclosure. Values marked N/A exceed the parameters for the task tables and therefore the tables cannot be used.

When the NFPA 70E – 2018 PPE category method is used, the minimum arc rating of PPE was about 15 to 35 times higher than the incident energy measured during testing. This is illustrated in Figure 24.

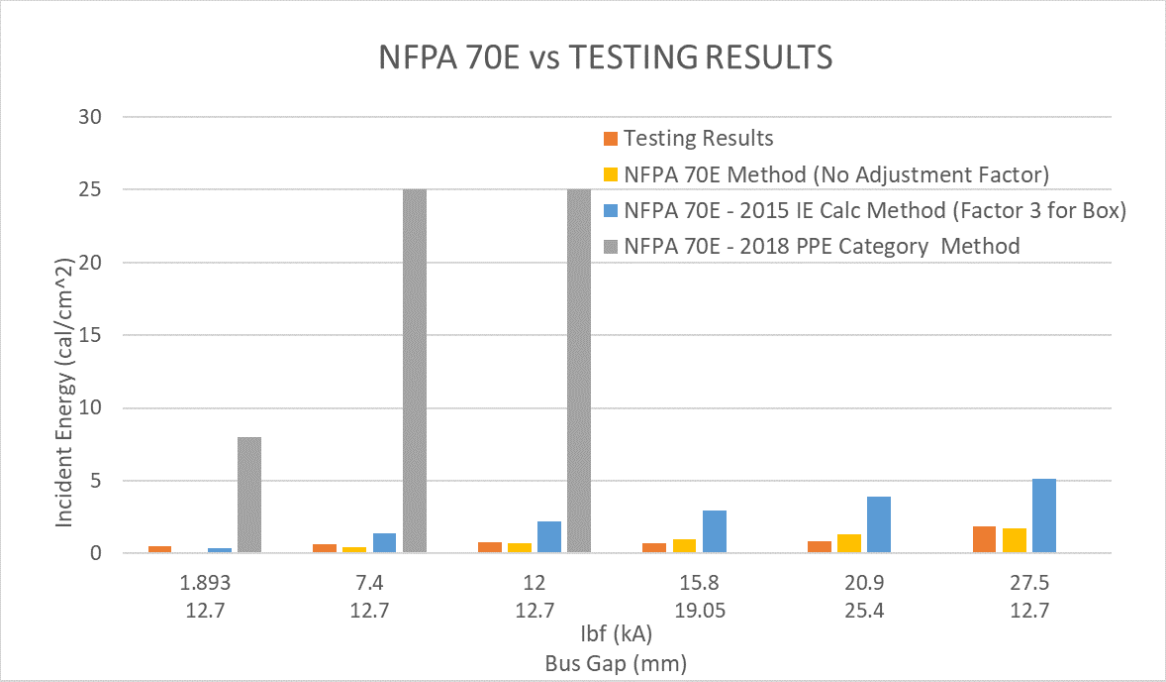

Figure 24 Incident Energy Comparison Between Measured Results and NFPA 70E 2015 and 2018 Methods Calculations were performed at bolted fault currents tested. Gap distance listed below fault current only applies to the test results, NFPA 70E methods do not consider bus gap in incident energy determination.

When using the incident energy calculation from informative annex D from NFPA 70E, the standard recommends that the task table be used and that PPE ratings selected be beyond what the table recommends resulting in even higher PPE incident energy ratings for arcs in an enclosure. This provides an even larger disparity between the recommended PPE and the test results. In addition, this recommendation effectively eliminates the incident energy analysis method when the arc occurs in an enclosure. The 2018 NFPA 70E also neglects to address situations where the fault current is beyond the PPE category method limits and the arc is in an enclosure. For cases that exceed the task tables, the incident energy calculation method is to be used; however, for DC systems it references the user back to the task tables. Since no recommendation is provided for cases that are above 15 kA, and are in an enclosure, to err on the side of caution would be to

prohibit work on the equipment while energized. Comparing the recommendation of the 2018 NFPA 70E to the actual test results yield of less than 2 cal/cm^2, at the maximum tested fault current of 27.5 kA, indicates that the use of the task tables for the incident energy calculation method for arcs in an enclosure should be reviewed based upon further testing. As seen in Figure 25, the 2015 method's highest minimum PPE rating was 5.13 cal/cm^2 at the 27.5 kA available fault current. This still indicates higher PPE requirements than the test results; however, it is not the drastic changes as seen by the 2018 edition.

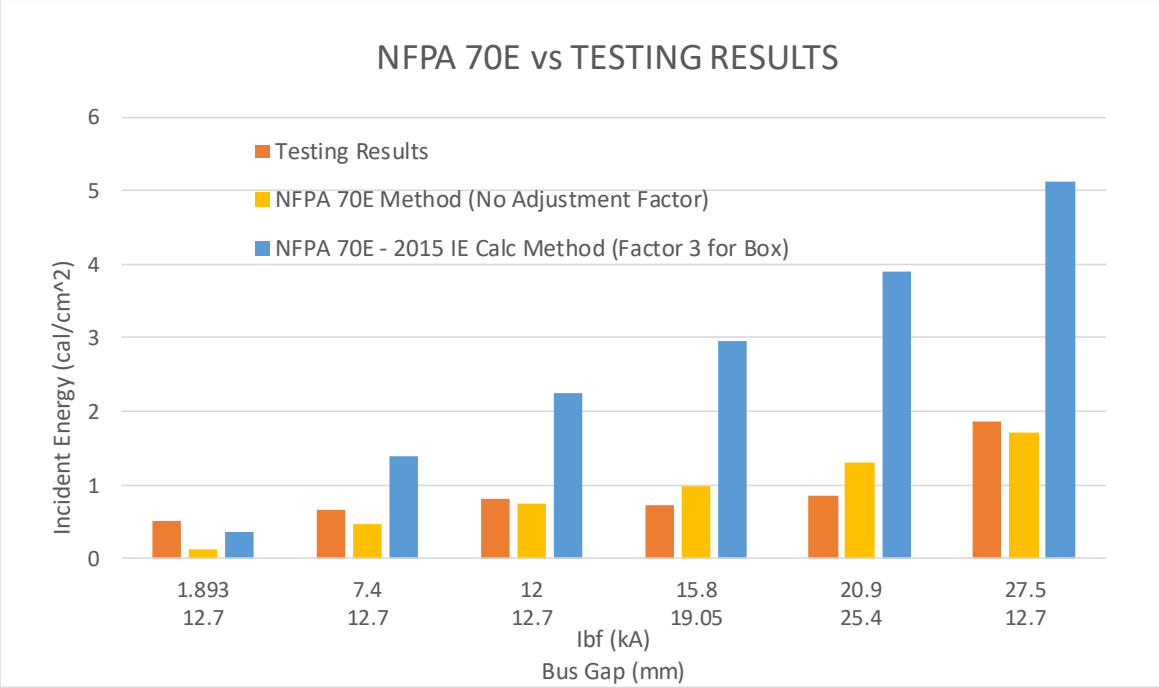

Figure 25 Incident Energy Comparison Between Measured Results and NFPA 70E 2015 and 2018 Methods (Excluding 2018 PPE Category Table Method)

Calculations were performed at bolted fault currents tested. Gap distance listed below fault current only applies to the test results, NFPA 70E methods do not consider bus gap in incident energy determination.

Typical arc formation is from the bottom of the electrodes and arc between the electrodes from the bottom, causing the arc to shoot downwards into the bottom of the enclosure and reflect outwards. In the VCCB configuration, however, this arc formation cannot occur resulting in arc formation just above the insulating barrier causing the arc to be directed more outwards than the typical VCB configuration, thus resulting in higher incident energy at the calorimeters. Even in this configuration, which should produce a higher incident energy, the measured results were at least a factor of ten less than the results calculated using the 2018 edition of the NFPA 70E standard. Also, the methods of this standard do not consider bus gap distance as a parameter, and therefore will produce incident energy values at gap distances where it was not possible to sustain an arc during testing.

The previous edition, NFPA 70E 2015, recommends multiplying the calculated incident energy using (3-2) by a factor of three (3) for enclosures. Since our testing was done inside the box, this recommended factor was applied. As a result, the calculated values were about 2 to 4.5 times higher than those obtained from testing. Except for the test case of 12.7 mm (0.5 in) gap at 1.893 kA bolted fault current, which has about half of the measured incident energy. The largest disparities for the other tests were the 20.9 kA and 15.8 kA tests where the gap distances were at 19.05 mm (0.75 in) and 25.4 mm (1 in) respectively, which would produce lower incident energies than if the gap was 12.7 mm (0.5 in), as seen with the other fault current levels. Assuming the incident energy increased at 12.7 mm (0.5 in) gap, the disparity between this method and the measured results would be closer to a factor of two. However, since the maximum fault current from testing was not at the 12.7 mm (0.5 in) gap it clearly illustrates the importance that gap distance has on incident energy levels. In addition, if performing a study with equipment that has a 63.5 mm (2.5 in) gap distance, the 2015 NFPA 70E method would still yield 2.24 cal/cm^2, as it

did for the 12.7 mm (0.5 in) gap at 12 kA. However, during testing it was not possible to sustain an arc at the 63.5 mm (2.5 in) gap distance.

Disregarding the 2015 and 2018 NFPA 70E adjustments of (3-2) for arc in an enclosure, the results calculated using (3-2) are consistently lower than the measured values with tests that had a bus gap of 12.7 mm (0.5 in). As mentioned previously, the NFPA 70E equation does not consider gap distance, and therefore as the testing gap distance changed the disparity of the results increased and decreased. The largest disparity between the measured values and (3-2) was the testing at 1893 A fault current. The measured result was over four times the estimate of (3-2). However, the other results were generally much closer to the measured value with the result from (3-2) being half to 1.5 times the measured value. Unfortunately, the results from (3-2) were under the measured values when the gap distances were 12.7 mm (0.5 in) which would fail to adequately protect the worker from the incident energy. The instances that (3-2) was above the measured values were when the gap distances were 19.05 mm (0.75 in) and 25.4 mm (1 in). Knowing that the incident energy increases when the gap distance is reduced at 12.7 mm (0.5 in) it is unlikely that the results from (3-2) would still remain above the test result. Based on these tests, it is clear that multiplying by a factor of three in the 2015 edition was a wise decision.

3.4.2 Arc Current Magnitude Comparison of NFPA 70E and Experimental Results

The NFPA 70E method estimates the arcing current to be half the bolted fault current as seen in (3-1). From testing the average measured arcing current ranged from 11 to 48% of the bolted fault current, as seen in Table 9. The disparity between the theoretical estimate and the measured arcing current increases at higher bolted fault currents. Seven (7) of the nine (9) tests were a quarter of the bolted fault current or less. Unsurprisingly, as seen in Table 9, the arcing current reduced as the gap distance increased.

Table 9 NFPA 70E Estimated I_{arc} vs Measured I_{arc}

Test No.	Bus Gap (mm) [in]	I_{bf} (kA)	Measured Average I_{arc} (kA) [% I_{bf}]	Theoretical I_{arc} (kA)
2	12.7 [0.5]	12	3.00 [25%]	6
13	12.7 [0.5]	7.4	2.38 [32%]	3.7
15	12.7 [0.5]	1.893	0.91 [48%]	0.947
21	25.4 [1]	20.9	2.20 [11%]	10.45
22	25.4 [1]	20.9	3.25 [16%]	10.45
24	19.05 [0.75]	15.8	2.79 [18%]	7.9
26	25.4 [1]	15.8	2.49 [16%]	7.9
29	25.4 [1]	27.5	3.61 [13%]	13.75
30	12.7 [0.5]	27.5	5.20 [19%]	13.75

Theoretical I_{arc} is 50% of I_{bf} per (3-1).

Having an accurate estimation of the arcing current is essential for arc flash incident energy calculations. The magnitude of the arcing current is a key factor in determining the clearing time of the fault. If the arc current is sufficiently low the time to clear could be significantly higher than originally estimated, and could result in an even higher incident energy than originally estimated using (3-1) and (3-2).

3.4.3 Incident Energy Comparison of ETAP and Experimental Results

The testing data was also compared to the results obtained from ETAP and are consolidated in Table 10. As seen in Figure 26, the ETAP provided results were relatively close to measured values. Stokes and Oppenlander, and Paukert methods were consistently closer to the incident energy compared to the maximum power method. Their results never reaching twice that of the measured value. However, at the 1.893 kA and the 7.4 kA they were both below the measured value, being less than half for the 1.893 kA and being only 0.01 cal/cm^2 less than the measured for the 7.4 kA. The maximum power method had a similar problem at the 1.893 kA, being about 70% of the measured value. However, for all other test cases it was the highest result by far and ranged from 2 to 4.5 times as much as the measured values for the rest of the tests.

Table 10 Test Results and ETAP 19.5.0 Methods

I_{bf} (kA)	IE Measured (cal/cm^2)	Maximum Power (cal/cm^2)	Paukert (cal/cm^2)	Stokes & Oppenlander (cal/cm^2)
1.893	0.52	0.353	0.164	0.17
7.4	0.67	1.381	0.666	0.66
12	0.8	2.239	1.078	1.055
15.8	0.72	2.948	1.074	1.292
20.9	0.85	3.901	1.323	1.502
27.5	1.87	5.131	2.401	2.316

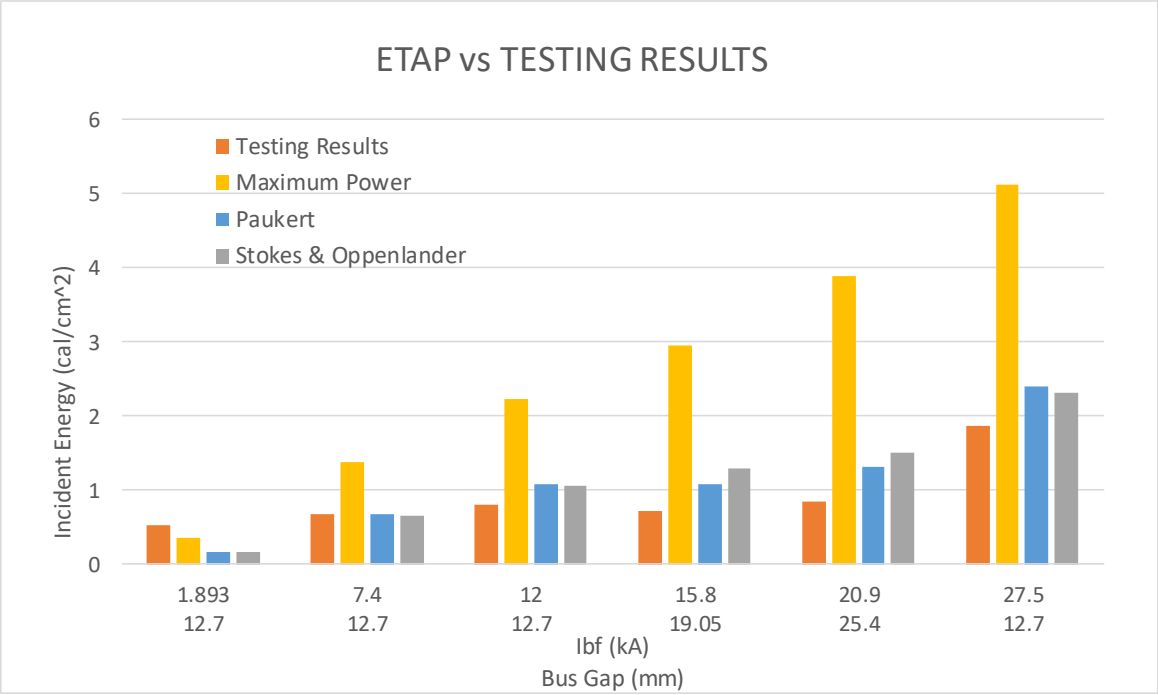

Figure 26 Incident Energy Comparison Between Measured Results and ETAP 19.5.0 Methods

Arc flash calculation methods (maximum power, Paukert, Stokes and Oppenlander) were performed at bolted fault currents tested. Gap distance listed below fault current does not apply to the maximum power method, which is independent of bus gap distance to determine incident energy.

4.0 Conclusion

In conclusion, the contribution of this work is to provide further public testing data of DC arc flash, including results of the sensitivity analysis of bus gap and fault current, and to provide a comparative analysis to current theoretical models. From testing it was observed that gap distance has a significant impact on DC arc sustainability and incident energy. The incident energy was found to be inversely proportional to gap distance. In one case, there was a 50% reduction of incident energy when the gap distance was increased from 12.7 to 25.4 mm (0.5 to 1 in). In addition, at gap distances greater than 25.4 mm (1 in), arc flash events were un-sustainable.

The incident energy results obtained from testing differ greatly from the maximum power models. The arc resistance models had some deviation, but were generally closer to the measured incident energies. Generally, these deviations were conservatively high, however, there were a few instances at low fault currents (1.893 kA) where the measured incident energy exceeded the theoretical models.

This testing performed and the deviations seen between the measured results and the current theoretical models further cements the need for additional testing to be performed in regards to DC arc flash. The authors recommend that an IEEE standard be developed for DC arc flash. Alternatively, if DC arc flash could be added to IEEE 1584, with results based on testing as was done in this work, in order to update AC arc flash calculations in IEEE 1584 – 2018.

Appendix A Test Current and Voltage Waveforms

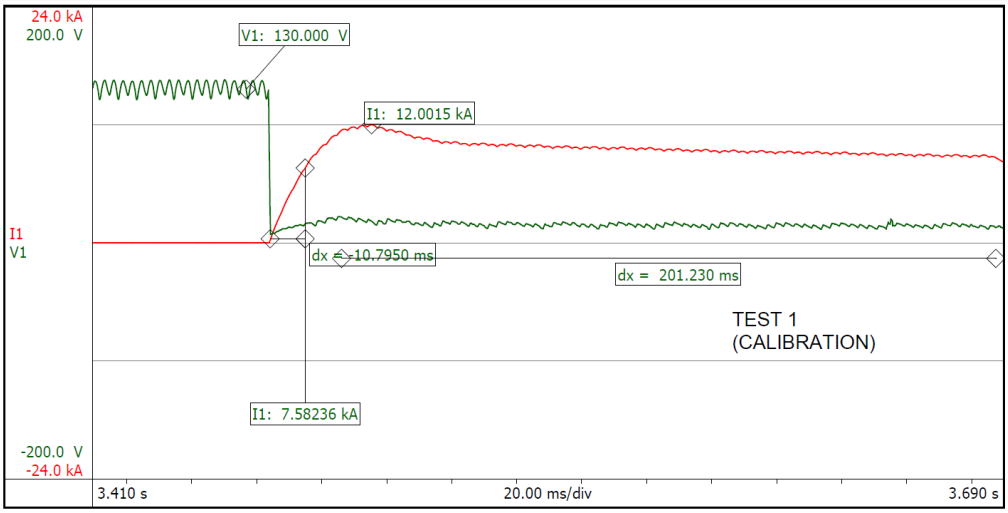

Appendix Figure 1 Test 1 Current and Voltage Waveforms

Calibration test, fault current (red) and voltage (green) waveforms. 10.7 ms time constant, and 12 kA bolted fault current.

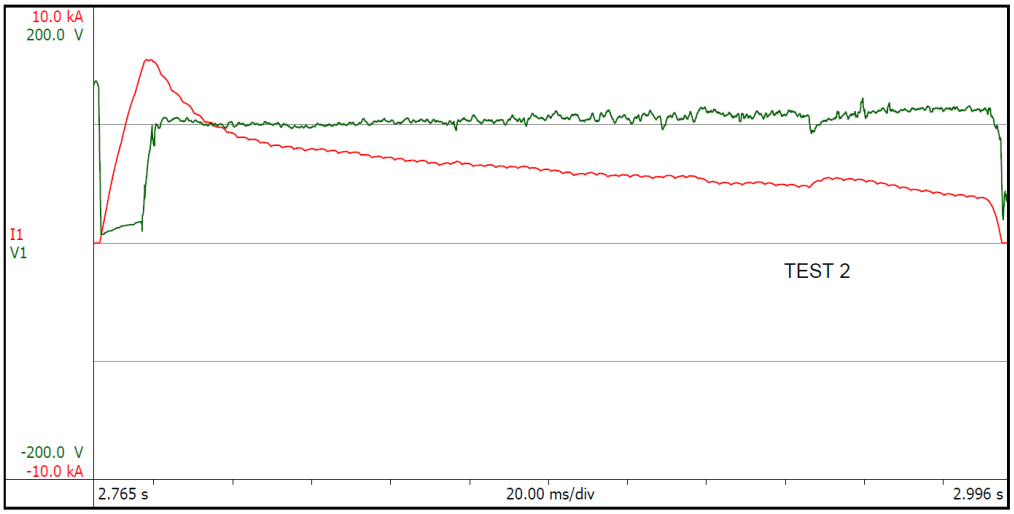

Appendix Figure 2 Test 2 Current and Voltage Waveforms

Sustained arc flash event, fault current (red) and voltage (green) waveforms. 12.7 mm (0.5 in) gap distance, 10.7 ms time constant, and 12 kA bolted fault current.

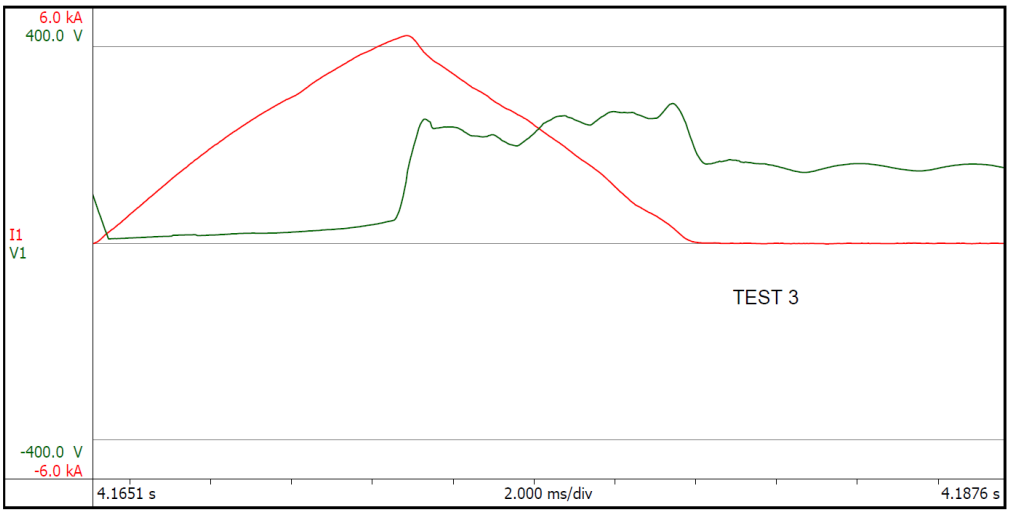

Appendix Figure 3 Test 3 Current and Voltage Waveforms

Un-sustained arc flash event, fault current (red) and voltage (green) waveforms. 63.5 mm (2.5 in) gap distance, 10.7 ms time constant, and 12 kA bolted fault current.

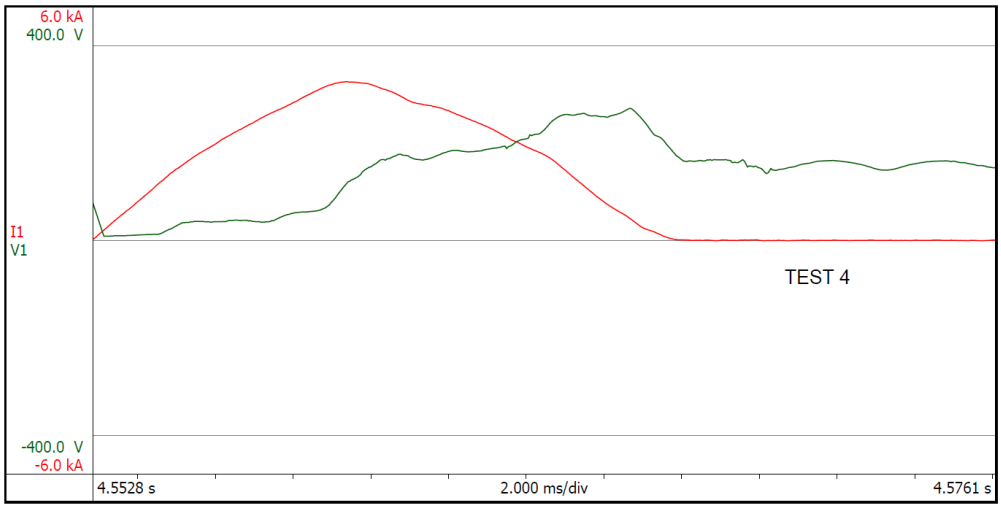

Appendix Figure 4 Test 4 Current and Voltage Waveforms

Un-sustained arc flash event, fault current (red) and voltage (green) waveforms. 63.5 mm (2.5 in) gap distance, 10.7 ms time constant, and 12 kA bolted fault current.

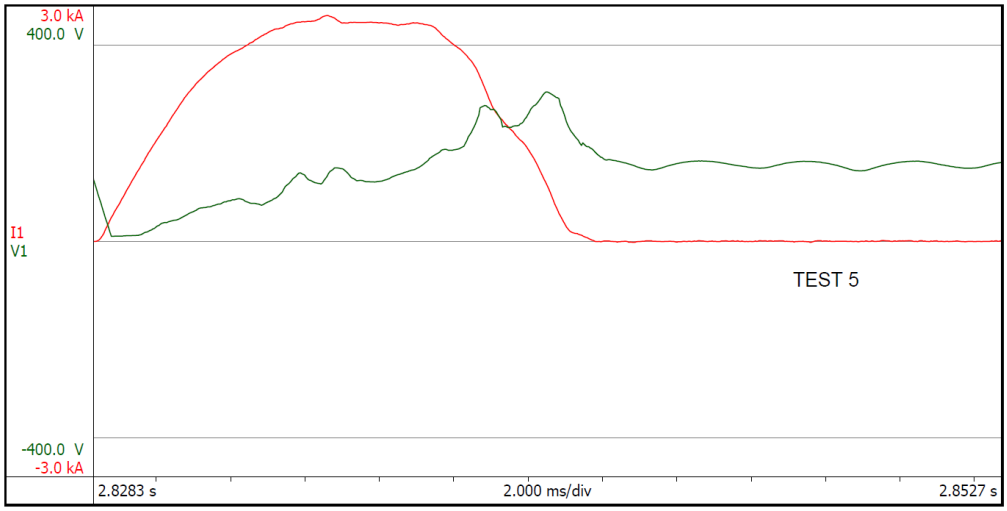

Appendix Figure 5 Test 5 Current and Voltage Waveforms

Un-sustained arc flash event, fault current (red) and voltage (green) waveforms. 63.5 mm (2.5 in) gap distance, 10.7 ms time constant, and 12 kA bolted fault current.

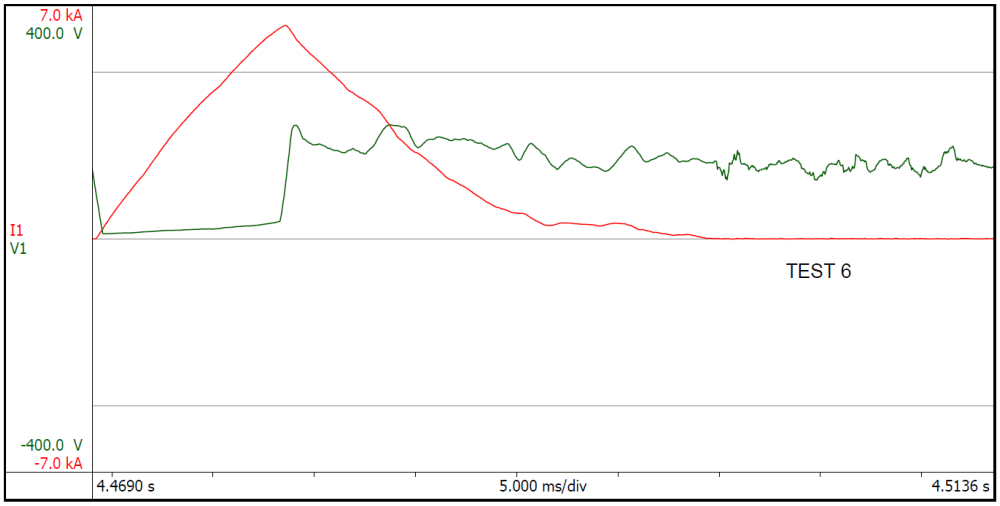

Appendix Figure 6 Test 6 Current and Voltage Waveforms

Un-sustained arc flash event, fault current (red) and voltage (green) waveforms. 38.1 mm (1.5 in) gap distance, 10.7 ms time constant, and 12 kA bolted fault current.

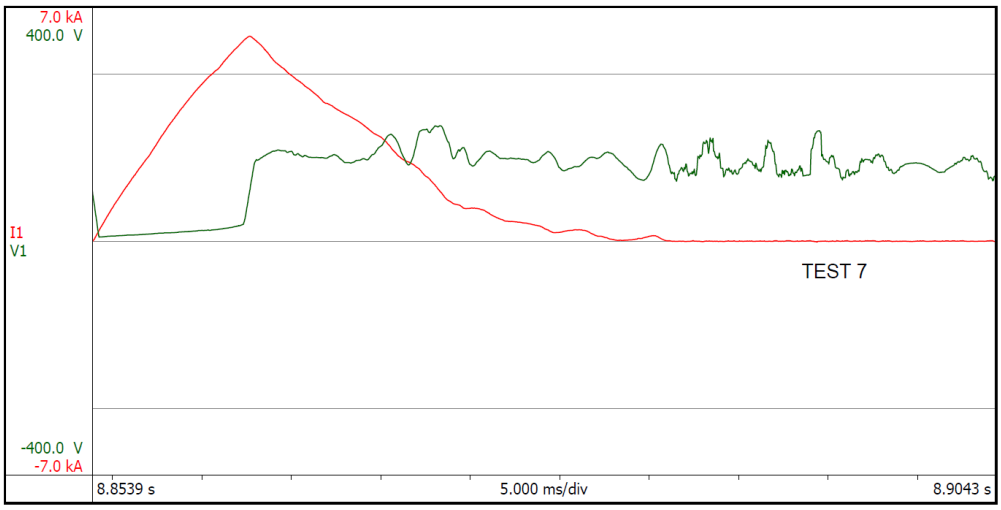

Appendix Figure 7 Test 7 Current and Voltage Waveforms

Un-sustained arc flash event, fault current (red) and voltage (green) waveforms. 38.1 mm (1.5 in) gap distance, 10.7 ms time constant, and 12 kA bolted fault current.

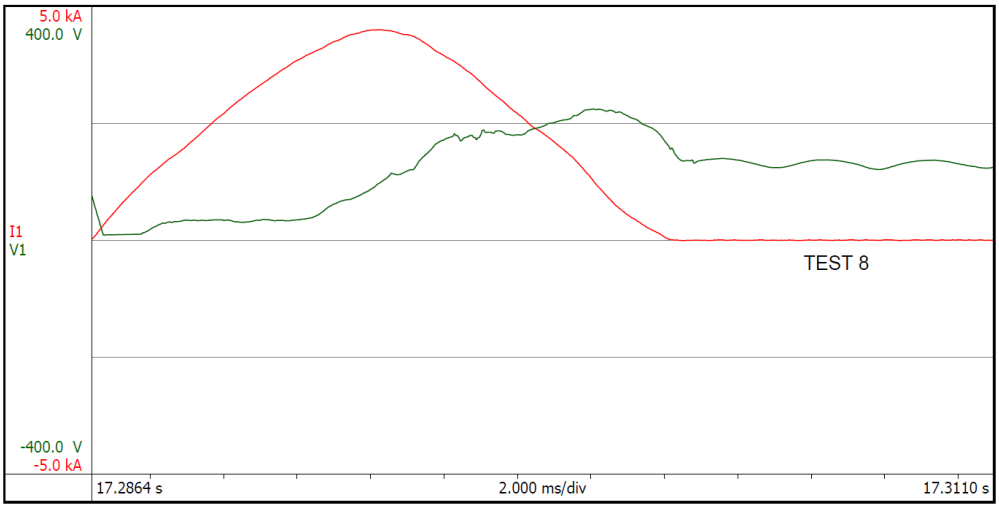

Appendix Figure 8 Test 8 Current and Voltage Waveforms

Un-sustained arc flash event, fault current (red) and voltage (green) waveforms. 38.1 mm (1.5 in) gap distance, 10.7 ms time constant, and 12 kA bolted fault current.

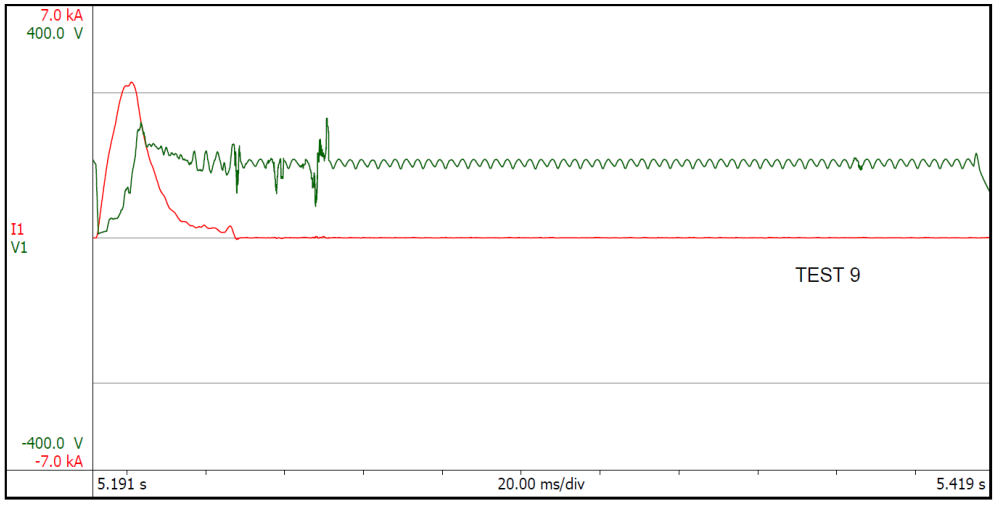

Appendix Figure 9 Test 9 Current and Voltage Waveforms

Un-sustained arc flash event, fault current (red) and voltage (green) waveforms. 25.4 mm (1 in) gap distance, 10.7 ms time constant, and 12 kA bolted fault current.

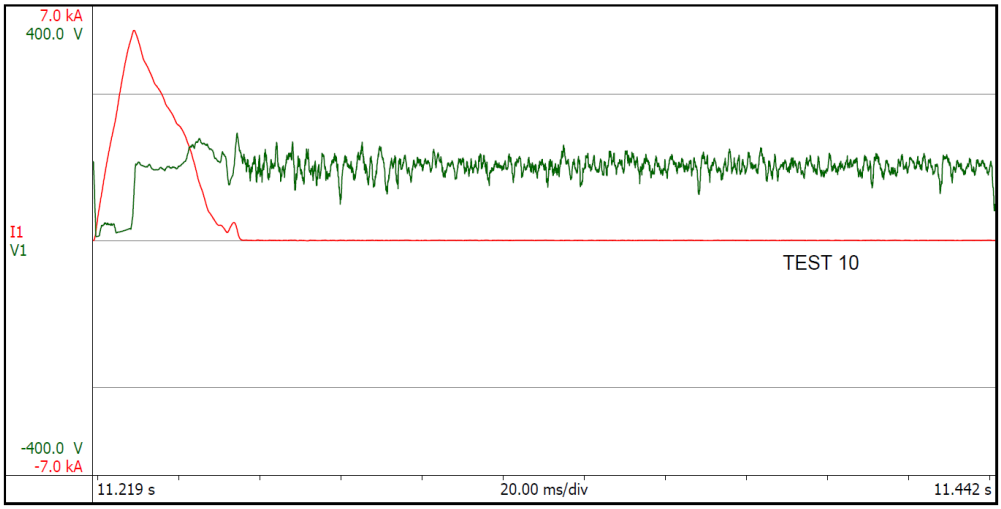

Appendix Figure 10 Test 10 Current and Voltage Waveforms

Un-sustained arc flash event, fault current (red) and voltage (green) waveforms. 25.4 mm (1 in) gap distance, 10.7 ms time constant, and 12 kA bolted fault current.

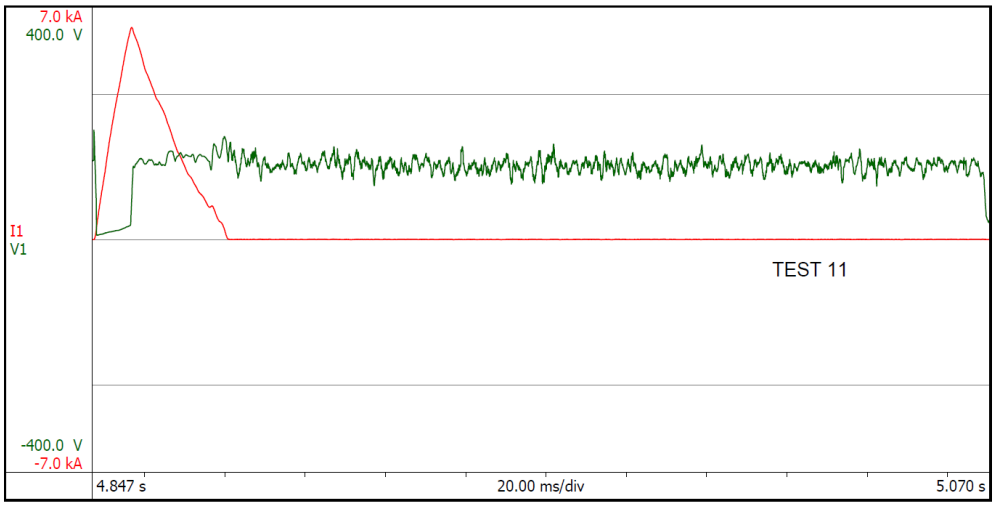

Appendix Figure 11 Test 11 Current and Voltage Waveforms

Un-sustained arc flash event, fault current (red) and voltage (green) waveforms. 25.4 mm (1 in) gap distance, 10.7 ms time constant, and 12 kA bolted fault current.

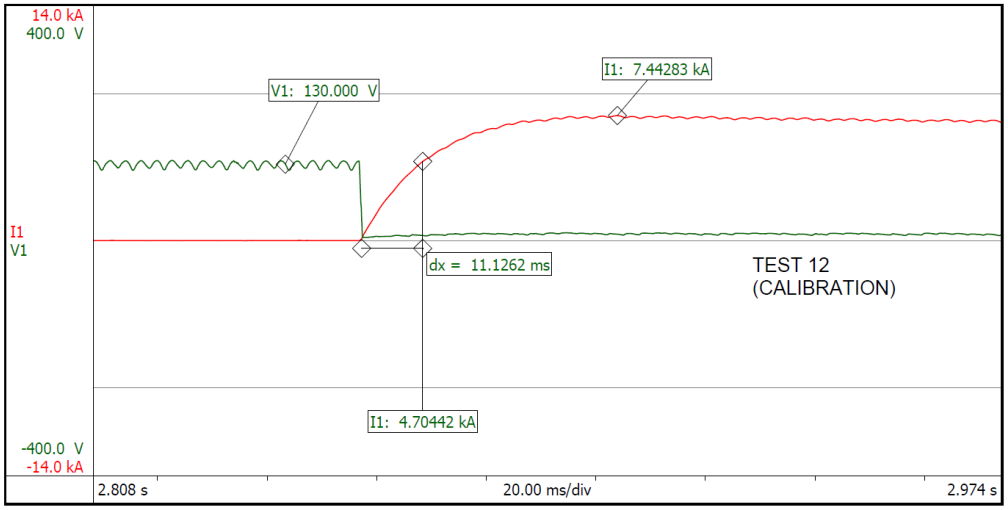

Appendix Figure 12 Test 12 Current and Voltage Waveforms

Calibration test, fault current (red) and voltage (green) waveforms. 11.1 ms time constant, and 7.4 kA bolted fault current.

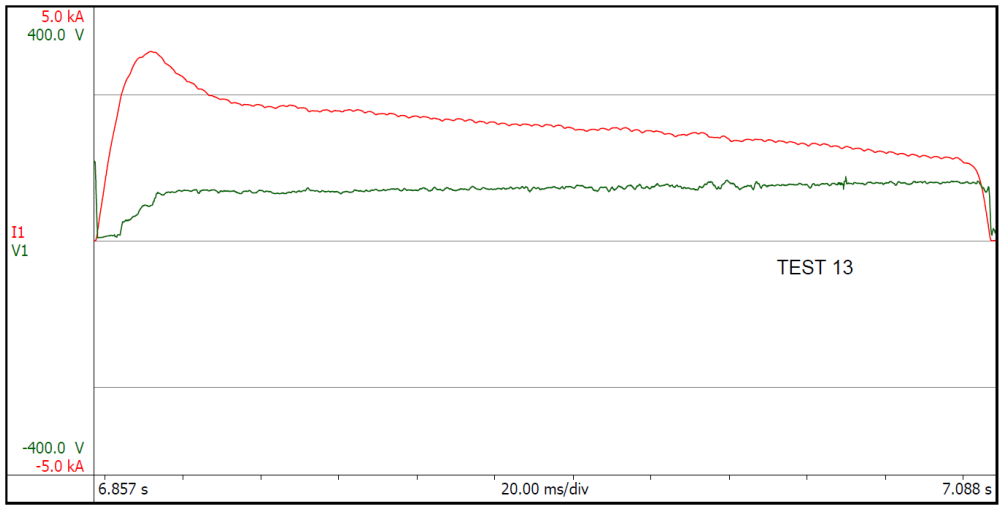

Appendix Figure 13 Test 13 Current and Voltage Waveforms

Sustained arc flash event, fault current (red) and voltage (green) waveforms. 12.7 mm (0.5 in) gap distance, 11.1 ms time constant, and 7.4 kA bolted fault current.

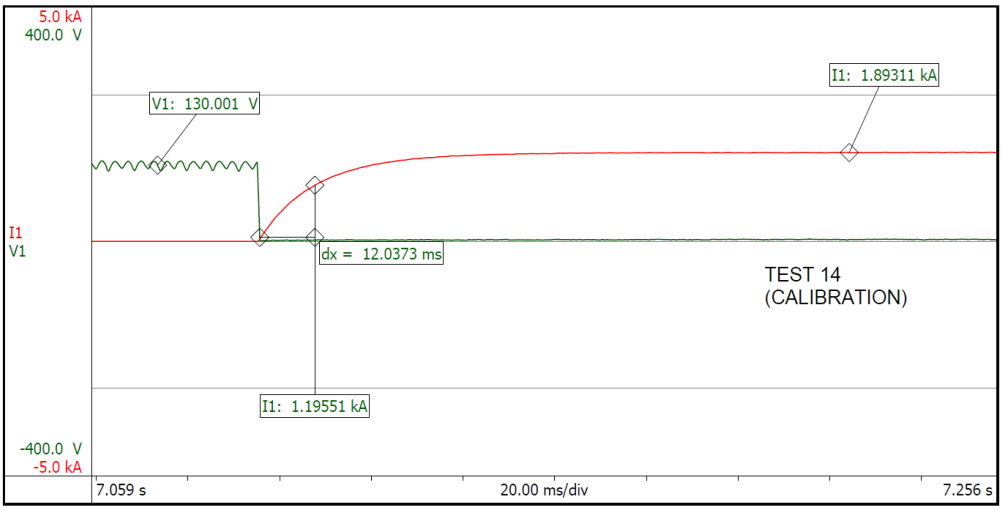

Appendix Figure 14 Test 14 Current and Voltage Waveforms

Calibration test, fault current (red) and voltage (green) waveforms. 12.03 ms time constant, and 1.893 kA bolted fault current.

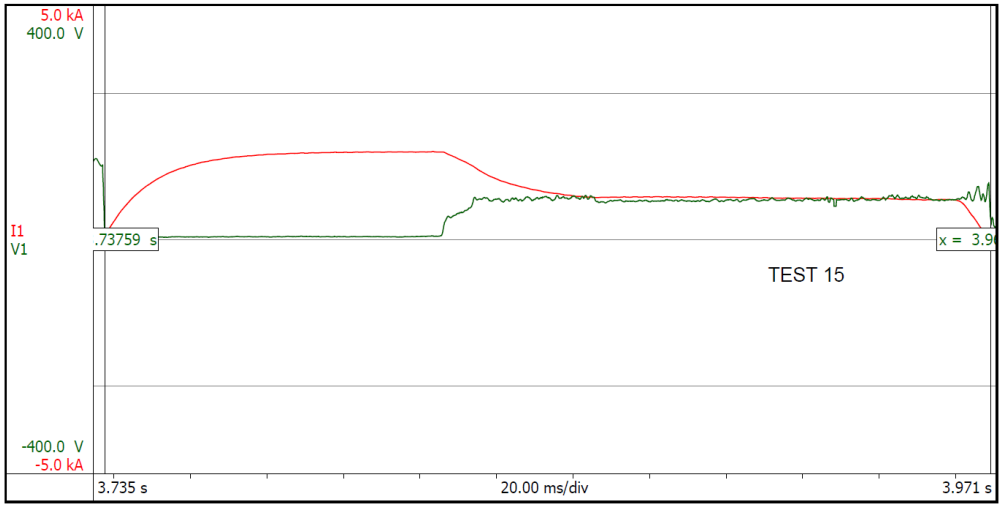

Appendix Figure 15 Test 15 Current and Voltage Waveforms

Sustained arc flash event, fault current (red) and voltage (green) waveforms. 12.7 mm (0.5 in) gap distance, 12.03 ms time constant, and 1.893 kA bolted fault current.

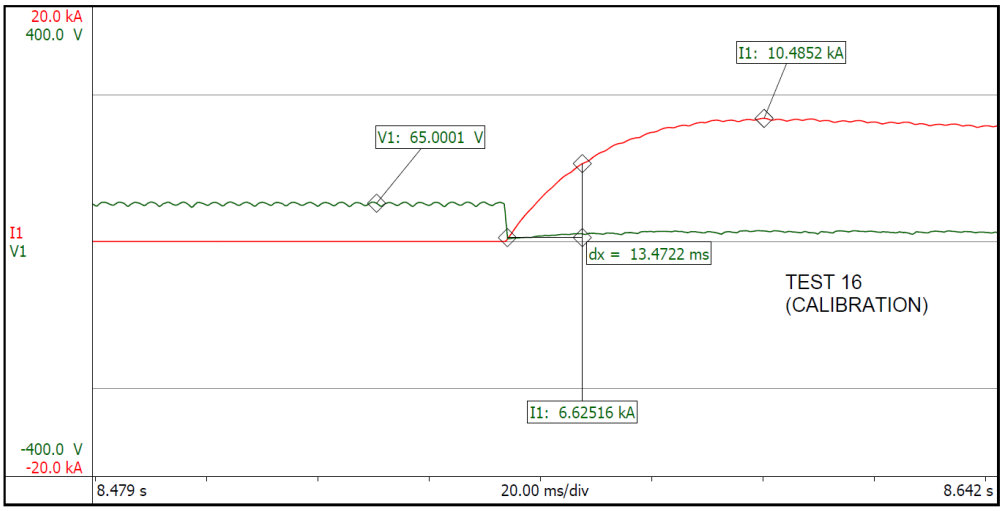

Appendix Figure 16 Test 16 Current and Voltage Waveforms

Calibration test, fault current (red) and voltage (green) waveforms. 13.47 ms time constant, and 20.9 kA bolted fault current.

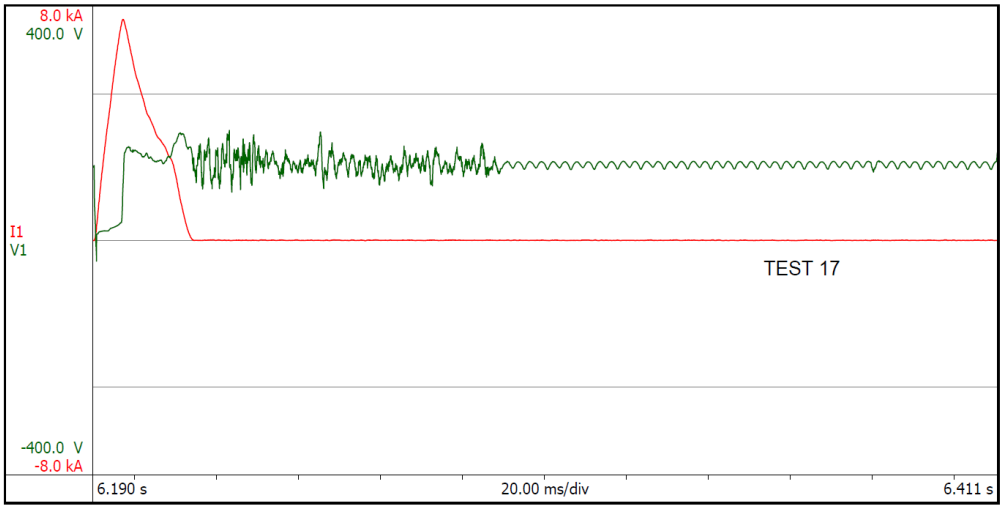

Appendix Figure 17 Test 17 Current and Voltage Waveforms

Un-sustained arc flash event, fault current (red) and voltage (green) waveforms. 38.1 mm (1.5 in) gap distance, 13.47 ms time constant, and 20.9 kA bolted fault current.

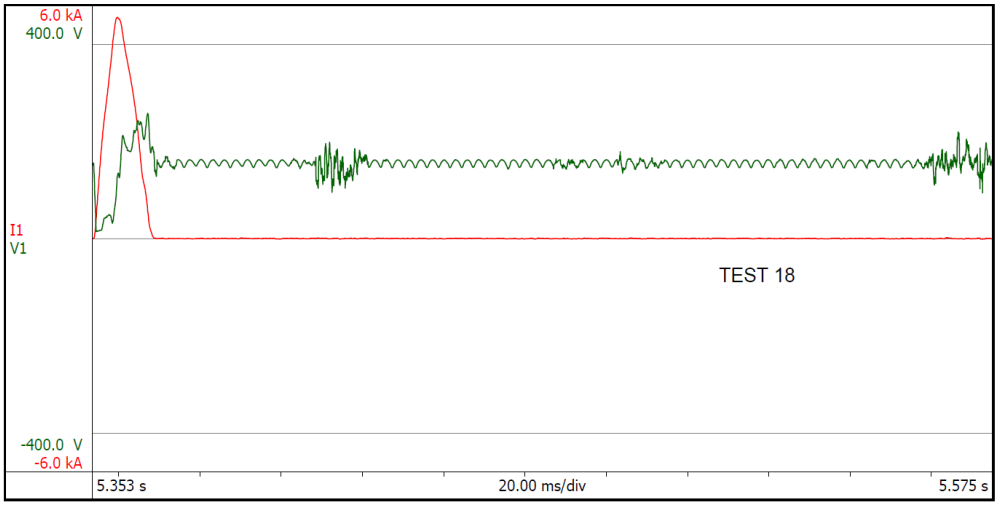

Appendix Figure 18 Test 18 Current and Voltage Waveforms

Un-sustained arc flash event, fault current (red) and voltage (green) waveforms. 38.1 mm (1.5 in) gap distance, 13.47 ms time constant, and 20.9 kA bolted fault current.

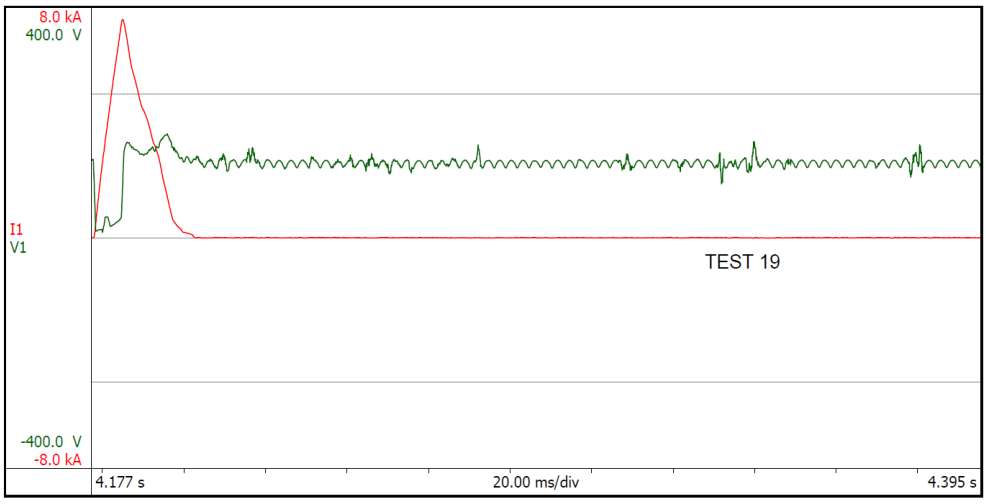

Appendix Figure 19 Test 19 Current and Voltage Waveforms

Un-sustained arc flash event, fault current (red) and voltage (green) waveforms. 38.1 mm (1.5 in) gap distance, 13.47 ms time constant, and 20.9 kA bolted fault current.

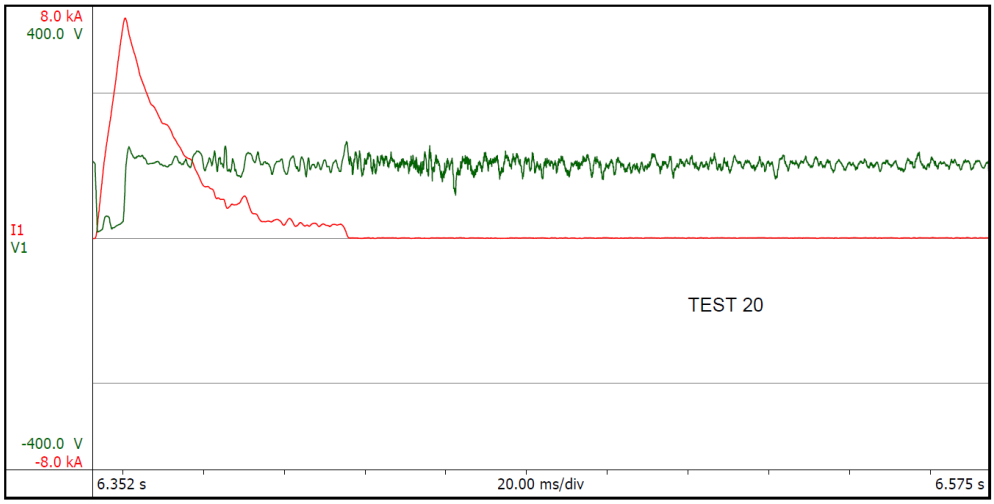

Appendix Figure 20 Test 20 Current and Voltage Waveforms

Un-sustained arc flash event, fault current (red) and voltage (green) waveforms. 25.4 mm (1 in) gap distance, 13.47 ms time constant, and 20.9 kA bolted fault current.

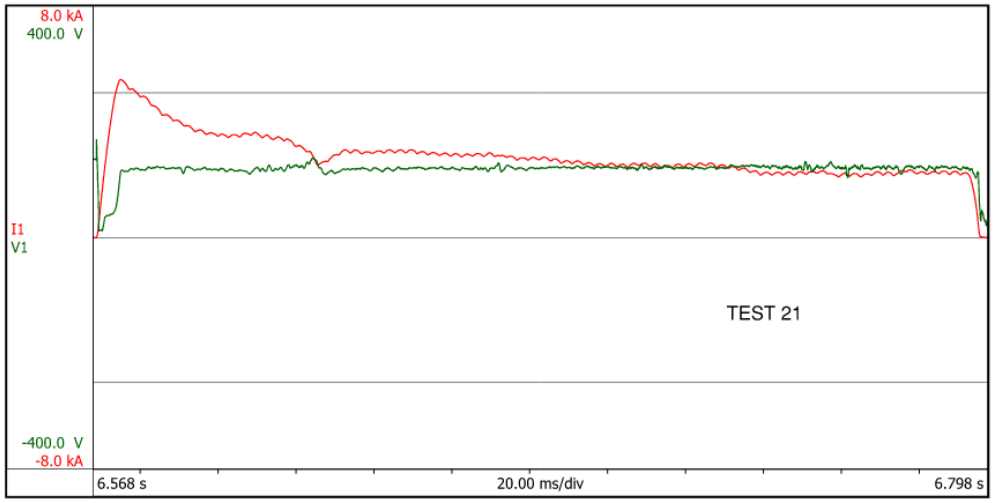

Appendix Figure 21 Test 21 Current and Voltage Waveforms

Sustained arc flash event, fault current (red) and voltage (green) waveforms. 25.4 mm (1 in) gap distance, 13.47 ms time constant, and 20.9 kA bolted fault current.

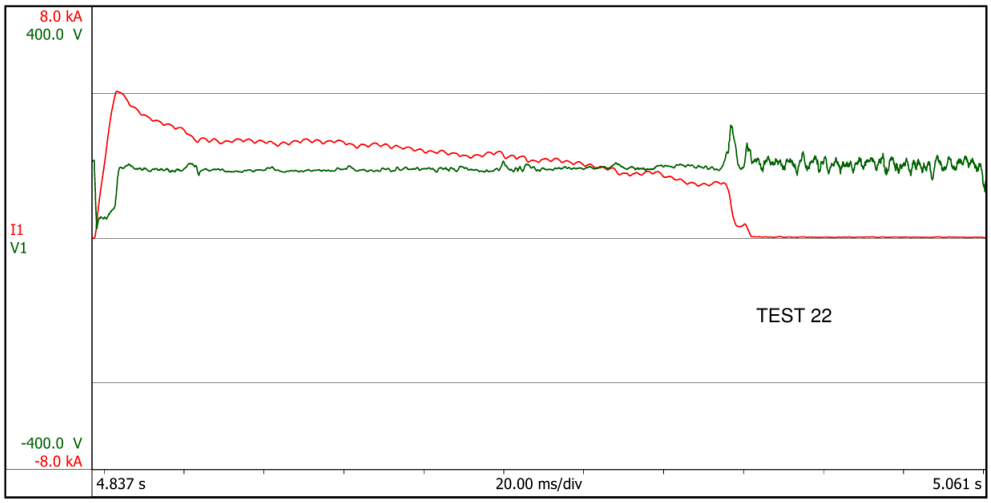

Appendix Figure 22 Test 22 Current and Voltage Waveforms

Sustained arc flash event, fault current (red) and voltage (green) waveforms. 25.4 mm (1 in) gap distance, 13.47 ms time constant, and 20.9 kA bolted fault current.

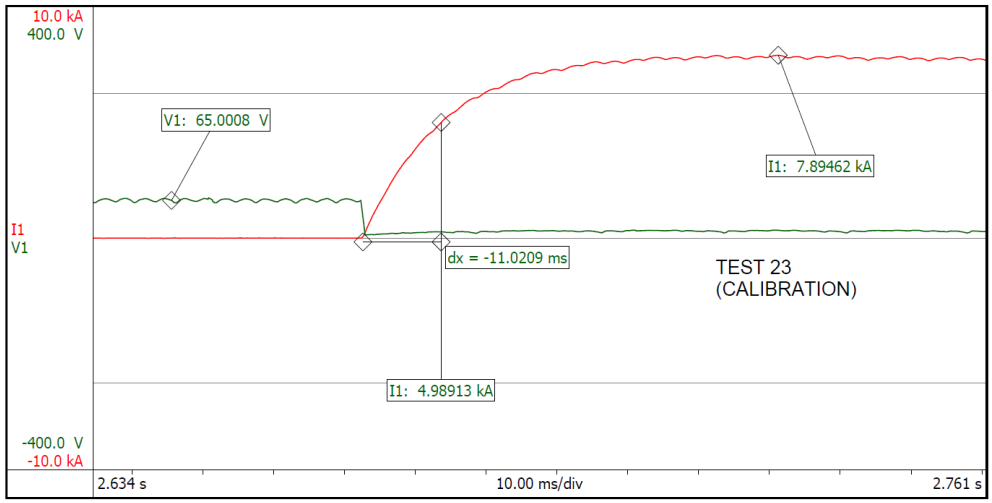

Appendix Figure 23 Test 23 Current and Voltage Waveforms

Calibration test, fault current (red) and voltage (green) waveforms. 11 ms time constant, and 15.8 kA bolted fault current.

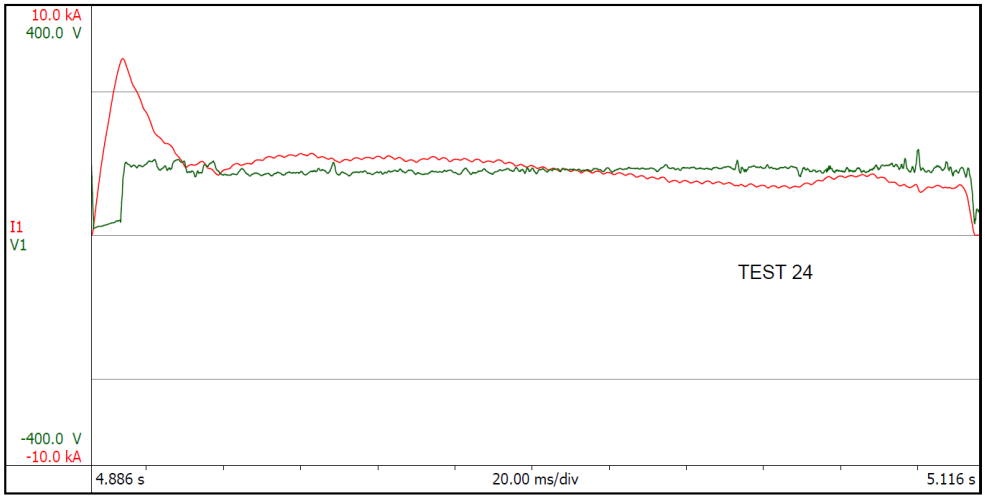

Appendix Figure 24 Test 24 Current and Voltage Waveforms

Sustained arc flash event, fault current (red) and voltage (green) waveforms. 19.05 mm (0.75 in) gap distance, 11 ms time constant, and 15.8 kA bolted fault current.

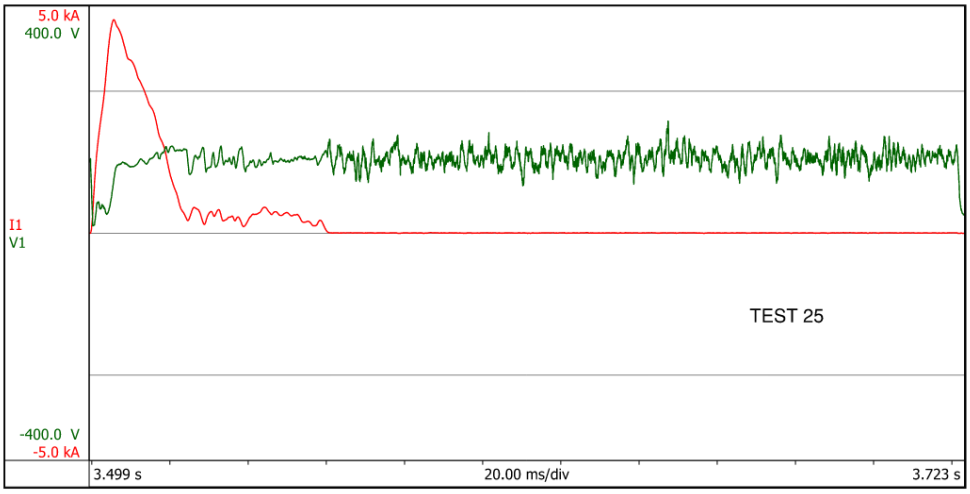

Appendix Figure 25 Test 25 Current and Voltage Waveforms

Un-sustained arc flash event, fault current (red) and voltage (green) waveforms. 25.4 mm (1 in) gap distance, 11 ms time constant, and 15.8 kA bolted fault current.

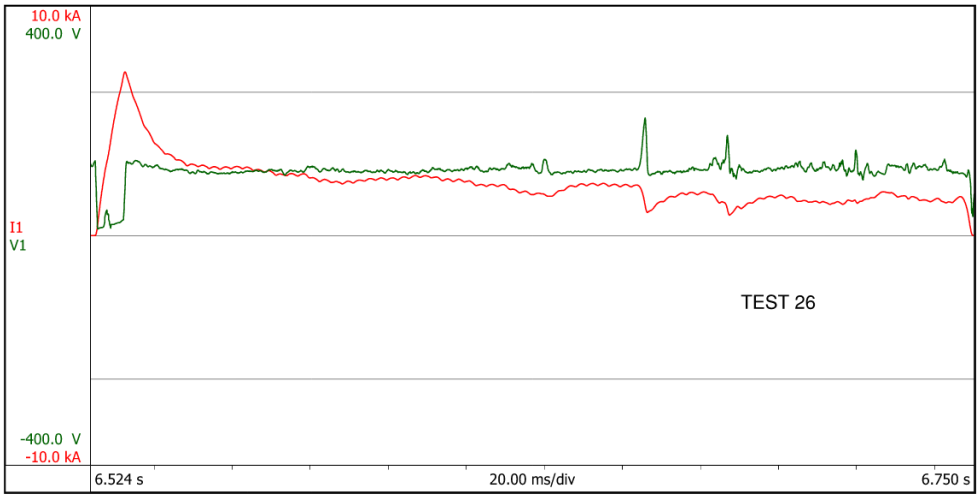

Appendix Figure 26 Test 26 Current and Voltage Waveforms

Sustained arc flash event, fault current (red) and voltage (green) waveforms. 25.4 mm (1 in) gap distance, 11 ms time constant, and 15.8 kA bolted fault current.

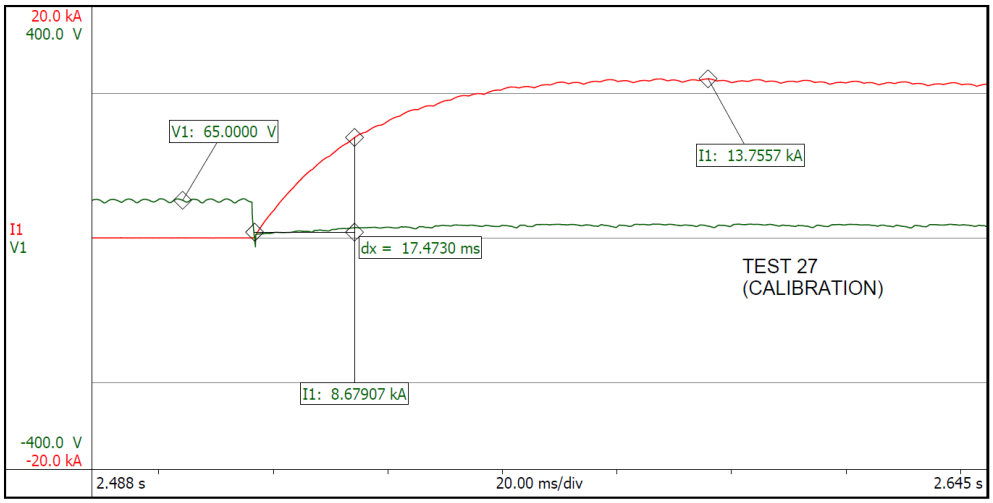

Appendix Figure 27 Test 27 Current and Voltage Waveforms

Calibration test, fault current (red) and voltage (green) waveforms. 17.4 ms time constant, and 27.5 kA bolted fault current.

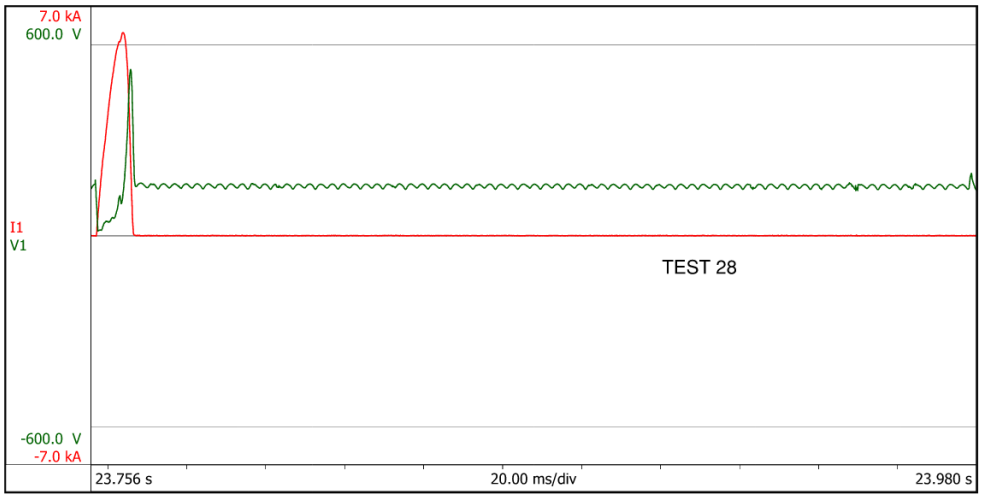

Appendix Figure 28 Test 28 Current and Voltage Waveforms

Un-sustained arc flash event, fault current (red) and voltage (green) waveforms. 25.4 mm (1 in) gap distance, 17.4 ms time constant, and 27.5 kA bolted fault current.

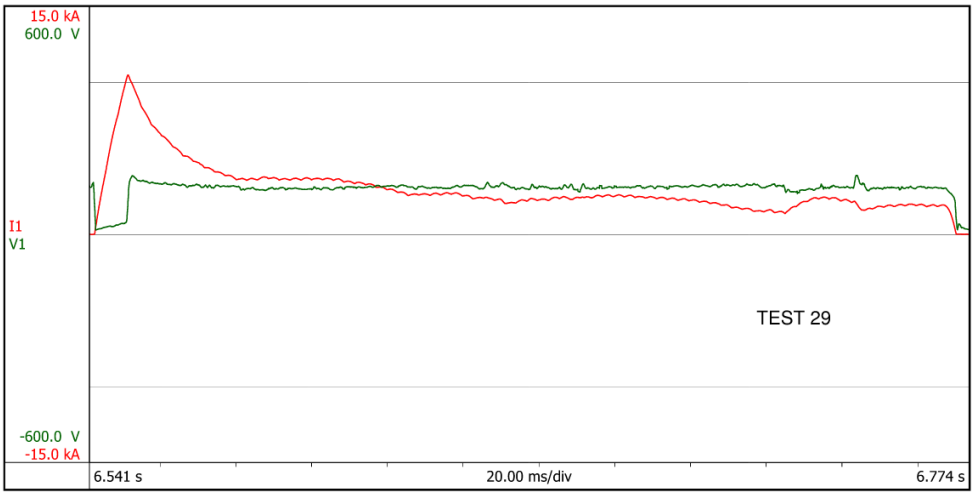

Appendix Figure 29 Test 29 Current and Voltage Waveforms

Sustained arc flash event, fault current (red) and voltage (green) waveforms. 25.4 mm (1 in) gap distance, 17.4 ms time constant, and 27.5 kA bolted fault current.

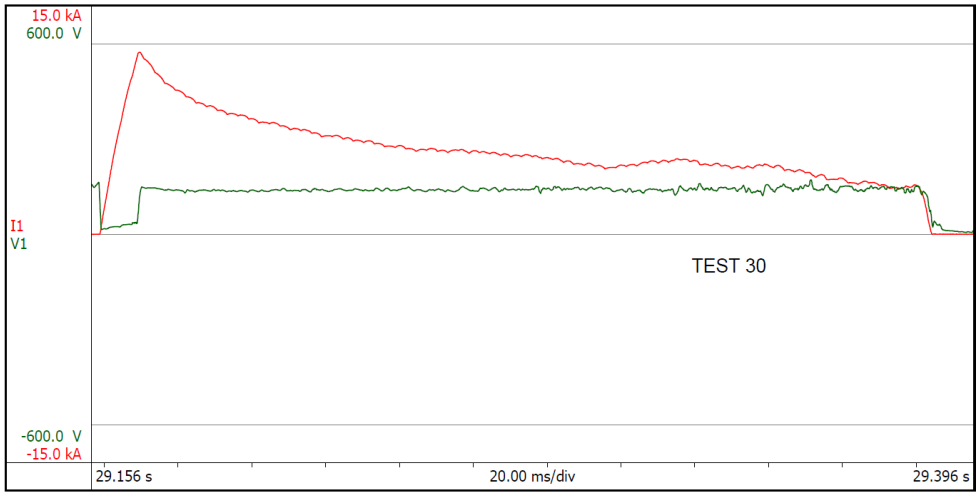

Appendix Figure 30 Test 30 Current and Voltage Waveforms

Sustained arc flash event, fault current (red) and voltage (green) waveforms. 12.7 mm (0.5 in) gap distance, 17.4 ms time constant, and 27.5 kA bolted fault current.

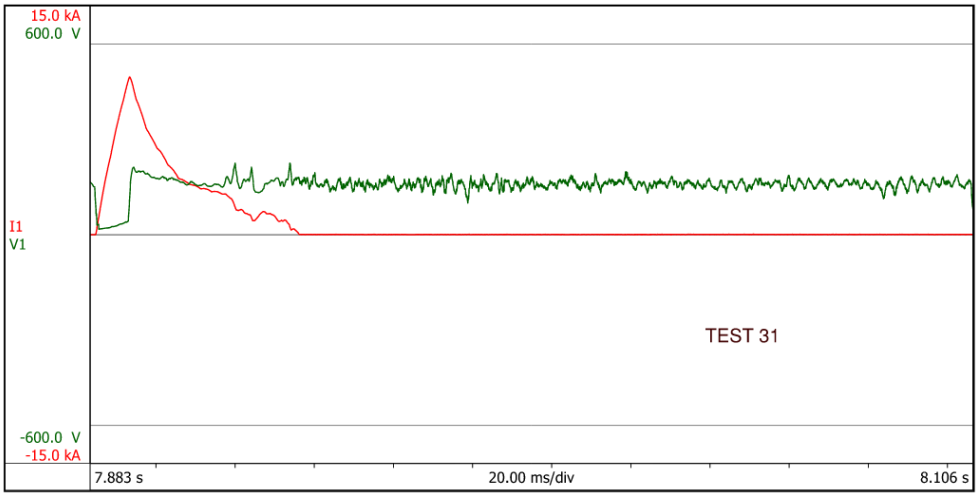

Appendix Figure 31 Test 31 Current and Voltage Waveforms

Un-sustained arc flash event, fault current (red) and voltage (green) waveforms. 38.1 mm (1.5 in) gap distance, 17.4 ms time constant, and 27.5 kA bolted fault current.

Bibliography

[1] IEEE Guide for Performing Arc-Flash Hazard Calculations, IEEE Standard 1584, 2018.

[2] R. Campbell. (2018, May). “Fatal electrical injuries at work”. [Online]. Available: https://www.nfpa.org/News-and-Research/Data-research-and-tools/Electrical/Fatal-electrical-injuries-at-work

[3] Regulations (Standards – 29 CFR), OSHA Standard 1910.

[4] Regulations (Standards – 29 CFR), OSHA Standard 1926.

[5] National Electrical Code, NFPA Standard 70, 2014.

[6] Standard for Electrical Safety in the Workplace, NFPA Standard 70E, 2018.

[7] K. S. Y. Cheng, S. L. Cress, and D. J. Minini, “Arc hazard assessment for DC applications in the transit industry,” *2011 APTA Rail Conf.*, Boston, MA, USA, Jun. 12-15, 2011, pp. 1-7.

[8] B. Paudyal, M. Bolen, T. Short and J. Woodard, "Measured and Calculated DC Arc-Flash Incident Energy in a Large-Scale Photovoltaic Plant," *IEEE Journal of Photovoltaics*, vol. 9, no. 5, pp. 1343-1349, Sept., 2019.

[9] *ETAP® 19.5 User Guide*, Operation Technology, Inc., Irvine, CA, USA, 2019.

[10] R. H. Lee, "The Other Electrical Hazard: Electric Arc Blast Burns," *IEEE Trans. Industry Applications*, vol. IA-18, no. 3, pp. 246-251, May 1982.

[11] IEEE Guide for Performing Arc-Flash Hazard Calculations, IEEE Standard 1584, 2002.

[12] *Power*Tools for Windows User’s Guide*, SKM Systems Analysis Inc., Manhattan Beach, CA, USA, April, 2019.

[13] *EasyPower Basic User Manual*, EasyPower LLC., Tualatin, OR, USA, June, 2020.

[14] T. Gammon, W. Lee, Z. Zhang and B. C. Johnson, "A Review of Commonly Used DC Arc Models," *IEEE Trans. Industry Applications*, vol. 51, no. 2, pp. 1398-1407, March-April, 2015.

[15] T. Gammon, W. Lee, Z. Zhang and B. C. Johnson, "“Arc Flash” Hazards, Incident Energy, PPE Ratings, and Thermal Burn Injury—A Deeper Look," in *IEEE Trans. Industry Applications*, vol. 51, no. 5, pp. 4275-4283, Sept.-Oct. 2015.

[16] J. Phillips. (2019, Feb). “Electrode configuration and 2018 IEEE 1584”. [Online].

[17] R. Wilkins, M. Allison and M. Lang, "Improved method for arc flash hazard analysis," *Conference, 2004 IEEE Industrial and Commercial Power Systems Technical*, Clearwater Beach, Florida, USA, 2004, pp. 55-62.

[18] R. L. Doughty, T. E. Neal and H. L. Floyd, "Predicting incident energy to better manage the electric arc hazard on 600-V power distribution systems," *IEEE Trans. Industry Applications*, vol. 36, no. 1, pp. 257-269, Jan.-Feb., 2000.

[19] R. Wilkins, M. Lang and M. Allison, "Effect of insulating barriers in arc flash testing," *Conference Record of 2008 54th Annual Pulp and Paper Industry Technical Conference*, Seattle, WA, 2008, pp. 120-125.

[20] D. R. Doan, "Arc Flash Calculations for Exposures to DC Systems," *IEEE Trans. Industry Applications*, vol. 46, no. 6, pp. 2299-2302, Nov.-Dec., 2010.

[21] 2017 National Electrical Safety Code(R) (NESC(R))," *2017 National Electrical Safety Code(R) (NESC(R))*, vol., no., pp.1-405, 1 Aug., 2016.

[22] Standard for Electrical Safety in the Workplace, NFPA Standard 70E, 2015.

[23] H. C. Cline. (1995, April). Fuse protection of DC systems. Presented at American Power Conference Annual Meeting. [Online]. Available: https://arcadvisor.com/files/Fuse-Protection-of-DC-Systems.pdf

[24] R. F. Ammerman, T. Gammon, P. K. Sen and J. P. Nelson, "DC-Arc Models and Incident-Energy Calculations," *IEEE Trans. Industry Applications*, vol. 46, no. 5, pp. 1810-1819, Sept.-Oct., 2010.

[25] A. D. Stokes and W. T. Oppenlander, "Electric arcs in open air," Journal of Physiscs D: Applied Physics, 1991, vol. 24, pp. 26-35.

[26] K. Klement, "DC Arc Flash Studies for Solar Photovoltaic Systems: Challenges and Recommendations," *IEEE Trans. Industry Applications*, vol. 51, no. 5, pp. 4239-4244, Sept.-Oct., 2015.

[27] J. Yuventi, "DC Electric Arc-Flash Hazard-Risk Evaluations for Photovoltaic Systems," *IEEE Trans. Power Delivery*, vol. 29, no. 1, pp. 161-167, Feb., 2014.

[28] E. H. Enrique, P. N. Haub and T. P. Bailey, "DC Arc flash calculations for solar farms," *2013 1st IEEE Conference on Technologies for Sustainability (SusTech)*, Portland, OR, 2013, pp. 97-102.

[29] P. Brucke and M. Manjarekar, "DC arc flash risk assessments for photovoltaic systems," *2016 IEEE 43rd Photovoltaic Specialists Conference (PVSC)*, Portland, OR, 2016, pp. 3234-3236.

[30] D. C. Jordan and S. R. Kurtz, "Photovoltaic Degradation Rates – An Analytical Review," NREL/JA-5200-51664, June, 2012.

[31] ArcPro™ Software, Kinectrics Inc., Toronto, ON, Canada.

[32] J. Paukert, “The arc voltage and arc resistance of lv fault arcs," *Proc. 7th Int. Symp. Switching Arc Phenom.*, 1993, pp. 49-52.

[33] Standard Test Method for Determining the Arc Rating of Materials for Clothing, ASTM Standard F1959/M1959 – 14, 2014.

[34] Switchboards, UL Standard 891, 2019.